Anomaly detection search for new resonances decaying into a Higgs boson and a generic new particle X in hadronic final states using $\sqrt{s} = 13$ TeV pp collisions with the ATLAS detector

G. Aad *et al.*[*]

(ATLAS Collaboration)

A search is presented for a heavy resonance Y decaying into a Standard Model Higgs boson H and a new particle X in a fully hadronic final state. The full Large Hadron Collider run 2 dataset of proton-proton collisions at $\sqrt{s} = 13$ TeV collected by the ATLAS detector from 2015 to 2018 is used and corresponds to an integrated luminosity of 139 fb^{-1}. The search targets the high Y-mass region, where the H and X have a significant Lorentz boost in the laboratory frame. A novel application of anomaly detection is used to define a general signal region, where events are selected solely because of their incompatibility with a learned background-only model. It is constructed using a jet-level tagger for signal-model-independent selection of the boosted X particle, representing the first application of fully unsupervised machine learning to an ATLAS analysis. Two additional signal regions are implemented to target a benchmark X decay into two quarks, covering topologies where the X is reconstructed as either a single large-radius jet or two small-radius jets. The analysis selects Higgs boson decays into $b\bar{b}$, and a dedicated neural-network-based tagger provides sensitivity to the boosted heavy-flavor topology. No significant excess of data over the expected background is observed, and the results are presented as upper limits on the production cross section $\sigma(pp \to Y \to XH \to q\bar{q}b\bar{b})$ for signals with m_Y between 1.5 and 6 TeV and m_X between 65 and 3000 GeV.

I. INTRODUCTION

The Standard Model (SM) provides a framework for understanding fundamental particles and interactions that has been remarkably predictive of experimental results over several decades. The discovery of the Higgs boson in 2012 [1,2] completed the set of particles predicted by the SM.

The sensitivity of the Higgs boson mass to radiative corrections implies either extreme fine-tuning in the SM or the existence of new particles at an energy scale not far above the Higgs boson mass. This theoretical motivation, coupled with the existing experimental mass reach of the Large Hadron Collider (LHC) at CERN, motivates searches for new particles with $\mathcal{O}(\text{TeV})$ masses. Because the Higgs boson couples more strongly to heavier particles, it is natural to expect that these new heavy particles may have decays to a Higgs boson.

A search is presented here for a new TeV-scale narrow-width particle Y, which decays into a Standard Model Higgs boson H and a new particle X with a mass near the weak scale. A fully hadronic final state is targeted for both particles. Tagging of the boosted Higgs decay into two b quarks ($H \to b\bar{b}$ tagging) enhances a signal by using the highest branching fraction decay of the Higgs boson. A novel jet-level implementation of *anomaly detection* implemented via an unsupervised machine-learning architecture is used to select X particles solely because of their incompatibility with the expected SM background.

The application of anomaly detection to collider searches is a rapidly growing effort in the high-energy physics community (see Refs. [3–5] for overviews). The lack of evidence for new interactions and particles since the Higgs boson's discovery has motivated the execution of generic searches to complement the existing rigorous, model-dependent analysis program. Machine learning provides an excellent framework for the construction of tools that can isolate events in data solely because of their incompatibility with a background-only hypothesis. Building a tool to perform model-independent classification of collision events involves training on data events and, therefore, requires the ability to cope with a lack of labels indicating whether inputs are signal or background.

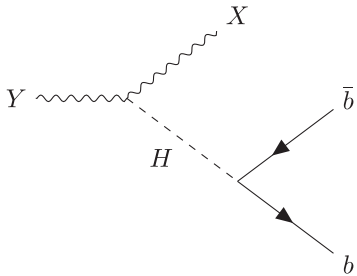[*]Full author list given at the end of the article.

FIG. 1.   Feynman diagram of the target signal process, where the Y is produced in the initial pp collision and decays to a fully hadronic final state via a SM Higgs boson $H \to b\bar{b}$ and a new particle X. The only assumption applied to the X decay is that it yields a hadronic final state.

This distinguishes the typical supervised classification problem, where all inputs are labeled with a known origin, from the anomaly detection approach, which makes use of unsupervised (no input labels) or weakly supervised (noisy labels) training. A selection tool that is constructed in this way has trade-offs: while it broadens sensitivity to many classes of new physics with a single classifier, it is expected that sensitivity to any specific model will be better with a dedicated supervised approach.

A Feynman diagram for the $Y \to XH$ signal process is shown in Fig. 1, where the X can have a variety of hadronic decays. A nominal benchmark decay into two light quarks, $X \to q\bar{q}$, is generated to provide an interpretation framework for the results. The generic selection of the X is not strongly dependent on its mass, so the analysis is sensitive to X masses spanning several orders of magnitude, from $\mathcal{O}(10)$ GeV to $\mathcal{O}(1)$ TeV. The masses of the parent and daughter particles yield a kinematic scenario where the final-state particles are highly Lorentz-boosted in the laboratory frame, motivating a "boosted" reconstruction method using large-radius (large-R) jets and jet substructure observables to distinguish the boson decay products. An orthogonal "resolved" reconstruction method is used to recover sensitivity to topologies where the X is less boosted and reconstructed as separate small-radius (small-R) jets, significantly extending the sensitive phase-space region. Since the signal is resonant, it can be detected with a "bump hunt" on the invariant mass distribution of the reconstructed X and H candidates.

Although model-independent in nature, this search is motivated by several key extensions to the Standard Model which predict heavy diboson resonances. Examples of such theories include extended gauge symmetry models [6], warped extra dimensions [7–9], or two-Higgs-doublet models [10]. Signals are generated with a simplified model based on spin-1 heavy vector triplets (HVT) [11] which reproduces a large class of explicit beyond-the-SM (BSM) models. The HVT phenomenology provides a Lagrangian that fulfills SM

symmetry constraints with an isospin SU(2) triplet formed of a neutral Z' and two charged $W'^{\pm}$ bosons.

This search uses the full LHC run 2 $\sqrt{s} = 13$ TeV pp dataset collected by the ATLAS detector from 2015 to 2018 and corresponding to an integrated luminosity of 139 fb^{-1}. A search for the $Y \to XH$ process was previously performed by ATLAS using 36.1 fb^{-1} of data, assuming $X \to q\bar{q}$, and found no significant excess for Y masses from 1 to 4 TeV and X masses from 50 to 1000 GeV [12]. In addition to the much larger dataset, the present analysis includes several key improvements relative to the previous search, such as a neural-network-based tagger optimized for the boosted $H \to b\bar{b}$ topology, anomaly detection for enhanced signal model independence, and the use of two orthogonal regions to capture both boosted and resolved reconstruction of the nominal X decay into two quarks. The ATLAS Collaboration previously leveraged anomaly detection implemented with weakly supervised machine learning in a search for narrow new resonances in dijet events using the full run 2 dataset [13]. The CMS experiment performed a multidimensional search for diboson resonances with their full run 2 dataset of 138 fb^{-1} which includes sensitivity to the signature discussed here [14]. A maximum local (global) significance of 3.6 (2.3) standard deviations was observed for two mild excesses of events, at resonance masses of 2.1 and 2.9 TeV with X masses consistent with W, Z, or Higgs bosons.

The analysis regions in the present search are built by selecting two large-R jets, with additional criteria to reduce the background to events with Higgs and X particles in the search regions. Three overlapping analysis categories are defined with different X selections, namely the anomaly region and two orthogonal regions optimized for the benchmark $X \to q\bar{q}$ decay. The degree of model independence of the X tagging is assessed using three simulated signals with different decays of the X particle that lead to differing large-R-jet topologies, in addition to the two-light-quark final state used to generate the (m_Y, m_X) signal grid. The background to the signal process consists primarily of multijet events from quantum chromodynamics (QCD) processes. It is estimated with a fully data-driven method that incorporates reweighting based on a deep neural network (DNN) to ensure good modeling. The final fits are made to the reconstructed invariant mass distribution of the Y candidates in overlapping ranges of X candidate mass to increase the sensitivity to a signal. Since no significant deviation from the estimated background is observed, results are presented as upper limits on the cross section times branching fraction for the generic HVT process.

II. ATLAS DETECTOR

The ATLAS detector [15] is a multipurpose particle detector with a forward-backward symmetric cylindrical

geometry and a near 4π coverage in solid angle.[1] The inner-detector (ID) system is immersed in a 2 T axial magnetic field and provides charged-particle tracking in the range $|\eta| < 2.5$. The high-granularity silicon pixel detector covers the vertex region and typically provides four space-point measurements per track, the first hit normally being in the insertable B layer installed before run 2 [16,17]. The next detector outward is the silicon microstrip tracker, which usually provides eight measurements per track. These silicon detectors are complemented by the transition radiation tracker, which enables radially extended track reconstruction up to $|\eta| = 2.0$. Lead and liquid-argon (LAr) sampling calorimeters provide electromagnetic (EM) energy measurements with high granularity. A steel and scintillator-tile hadron calorimeter covers the central pseudorapidity range ($|\eta| < 1.7$). The end cap and forward regions are instrumented with LAr calorimeters for both the EM and hadronic energy measurements up to $|\eta| < 4.9$. The muon spectrometer surrounds the calorimeters and is based on three large superconducting air-core toroidal magnets with eight coils each. The field integral of the toroids ranges between 2.0 and 6.0 Tm across most of the detector. The muon spectrometer includes a system of precision chambers for tracking and fast detectors for triggering. A two-level trigger system is used to select events. The first-level trigger is implemented in hardware and uses a subset of the detector information to accept events at a rate below 100 kHz on average depending on the data-taking conditions. This is followed by a software-based high-level trigger that reduces the rate of selected events to 1 kHz for offline storage. An extensive software suite [18] is used in data simulation, in the reconstruction and analysis of real and simulated data, in detector operations, and in the trigger and data acquisition systems of the experiment.

III. DATA AND MONTE CARLO SIMULATION

This search is performed with $\sqrt{s} = 13$ TeV pp collision data collected by the ATLAS detector during run 2 of the LHC (2015–2018). After the application of data quality requirements [19] to ensure that all detector components are operating normally, the dataset corresponds to an integrated luminosity of 139.0 ± 2.4 fb^{-1} [20,21]. Data events used in this analysis were triggered by the presence of a high-p_{T} large-R jet, built at trigger level using calorimeter-cell energy clusters calibrated to the hadronic scale utilizing the local cell-signal weighting

method [22]. The unprescaled single-large-R-jet trigger with the lowest jet-p_{T} threshold was used in each year, corresponding to thresholds of 360 GeV in 2015, 420 GeV in 2016, and 440 GeV in 2017 and 2018. Further offline selection criteria are imposed (see Sec. VI) to ensure that selected events are all in the kinematic region where the trigger is fully efficient.

Monte Carlo (MC) event generators were used to simulate the signal targeted by this search. The simulated event samples include the effect of additional pp interactions (pile-up) in the same or neighboring bunch crossings. The effect is assessed by overlaying simulated minimum-bias events on each hard-scatter event and accounting for how interactions in the previous or following bunch crossing affect the detector response. The simulated events are weighted to reproduce the pileup distribution observed in each data-taking period. The detector response was simulated [23] using Geant4 [24] and the events were reconstructed with the same software as used for data.

A generic HVT [11,25] model with simulated qq scattering is used as a baseline for the $Y \to XH$ signal samples. The Y resonance is assumed to have a width that is narrow compared to the detector resolution. The generation of the $W' \to WH$ process was modified to replace the W boson with a new spin-1 boson X with a width of 2 GeV and a 100% branching fraction to $u\bar{d}$. The Standard Model Higgs boson was generated with decays into $b\bar{b}$ only. Samples with Y resonance masses of 1–6 TeV were generated using MadGraph5_aMC@NLO 2.7.2 and 2.7.3 [26] interfaced to PYTHIA 8.2 [27] for parton showering and hadronization with the NNPDF2.3LO parton distribution function (PDF) set [28], at leading order in QCD, and parameter values set according to the A14 tune [29]. A two-dimensional grid was generated for 195 signal points defined by Y and X mass values, with Y masses in the range 1.5–6 TeV and X masses in the range 65–3000 GeV. The Y and X mass values account for the kinematic constraint $m_Y > m_X$, and the X mass boundaries are dictated by achievable sensitivity. The signal acceptance times the efficiency has values ranging from a few percent to 40% for the various signal region selections.

In addition to the $Y \to XH$ signal grid, three signals with different jet topologies were used to craft and assess the degree of model independence in the X anomaly-tagging procedure. They were all generated with PYTHIA 8 using the same tune (A14) and PDFs (NNPDF2.3LO) as the $Y \to XH$ signal grid. The HVT $W' \to WZ$ configuration from Ref. [30] was used to create generic resonance signatures of the form $A \to BC$, where the daughter particles decay into either three light quarks or two heavy-flavor quarks. Choosing as benchmarks a parent A mass of 3 TeV and daughter masses of 200 and 400 GeV creates approximately the same kinematic scenario as the $Y \to XH$ phase space of interest, leading to boosted decay products that are captured as large-R jets. Depending on the daughter decay

---

[1]ATLAS uses a right-handed coordinate system with its origin at the nominal interaction point (IP) in the center of the detector and the z axis along the beam pipe. The x axis points from the IP to the center of the LHC ring, and y axis points upward. Cylindrical coordinates (r, ϕ) are used in the transverse plane, ϕ being the azimuthal angle around the z axis. The pseudorapidity is defined in terms of the polar angle θ as $\eta = -\ln\tan(\theta/2)$.

into either qqq or $b\bar{b}$, the large-R jet is produced with three-prong substructure or displaced vertices, respectively. Lastly, the PYTHIA 8 hidden valley model A configuration was used to generate a "dark jet" signal that arises from the decay of a Z' dark sector mediator into two dark quarks, where the Z' has the same benchmark mass of 3 TeV [31]. These jets contain dark matter particles that do not interact with the detector, creating a hadronization pattern that contains both visible and invisible energy. Such jets are difficult to recognize using traditional substructure variables that focus on specific signal topologies, making them an ideal target for anomaly detection based on background-only characterization.

IV. OBJECT SELECTION

Charged-particle tracks measured to have $p_T > 500$ MeV in the inner detector are used to reconstruct pp collision vertices, and the one with the largest Σp_T^2 of such tracks is chosen as the event's primary vertex.

Jets are built with the anti-k_t algorithm [32] in FastJet [33], using two radius parameter values to cluster the constituent detector signals: $R = 1.0$ for large-R jets J and $R = 0.4$ for small-R jets j. Large-R jets must satisfy $p_T > 200$ GeV and $|\eta| < 2.0$. They are constructed from combinations of tracks and calibrated calorimeter energy clusters known as track-caloclusters (TCCs) [34]. The TCCs take advantage of both the excellent energy resolution of the ATLAS calorimeter and the better angular resolution of the ID tracking system at very high energy, where the calorimeter is less able to discern jet substructure. This is particularly advantageous for measuring substructure in highly boosted jets, as is needed in this search to distinguish $Y \to XH$ signal from multijet background. To minimize the impact of pile-up, large-R jets are trimmed [35] by removing any $R = 0.2$ subjets carrying less than 5% of the large-R jet's p_T. The jet energy and mass is calibrated with a MC-based method [36].

Small-R jets are built from particle-flow objects [37], with improved accuracy of the jet's charged-hadron energy component through measurements of the associated charged-particle momenta in the ID. Small-R jets must have $p_T > 20$ GeV and $|\eta| < 4.5$. An additional event-level veto is applied to reject events with a jet that is likely to have come from calorimeter noise, beam-induced background, or a cosmic ray [38].

Leptons, while excluded from the analysis region selections, participate in an overlap removal procedure that prevents double counting of overlapping objects. Leptons must have $p_T > 7$ GeV, with $|\eta| < 2.47$ for electrons and $|\eta| < 2.7$ for muons. To ensure that each lepton's track originates from the primary vertex, the transverse impact parameter d_0, measured relative to the beam line, must have a significance $|d_0/\sigma(d_0)| < 3(5)$ for muons (electrons), and the longitudinal impact parameter z_0, from the primary vertex to the point where d_0 is

measured, must satisfy $|z_0 \sin\theta| < 0.5$ mm. No lepton isolation criteria are applied.

The overlap removal procedure is applied to all selected leptons and jets. If two electrons share the same track, or the separation between their two energy clusters satisfies $|\Delta\eta| < 0.075$ and $|\Delta\phi| < 0.125$, then the lower-p_T electron is discarded. Electrons that fall within $\Delta R = 0.02$ of a selected muon are also discarded. For electrons and nearby small-R jets, the jet is removed if the separation between the electron and jet satisfies $\Delta R < 0.2$; the electron is removed if the separation satisfies $0.2 < \Delta R < 0.4$. For muons and nearby small-R jets, the jet is removed if the separation between the muon and jet satisfies $\Delta R < 0.2$ and if the jet has less than three tracks or the energy and momentum differences between the muon and the jet are small; otherwise the muon is removed if the separation satisfies $\Delta R < 0.4$. To prevent double counting of energy from an electron inside a large-R jet, the large-R jet is removed if its separation from the electron satisfies $\Delta R < 1.0$.

V. VARIATIONAL RECURRENT NEURAL NETWORK FOR ANOMALOUS-JET TAGGING

The anomaly detection in this search is performed with a jet-level anomaly score (S_A) [39]. The S_A value is given by a variational recurrent neural network (VRNN) [40], which consists of a variational autoencoder (VAE) whose latent space is updated at each time step of a recurrent neural network (RNN). The key features of this tool as it pertains to this analysis application are provided below, with a comprehensive description provided in Ref. [39].

The class of models that are based on autoencoders are popular for the selection of rare or outlier events in high-energy physics [41–46]. Such an architecture is composed of two separate stages: an encoder that compresses the input into a lower-dimensional latent space through identification of its salient features and a decoder that samples from the latent space and attempts to reproduce the input in its original dimensionality. Minimizing the reconstruction error between input and output is a key element of the training and allows the autoencoder to implicitly learn the underlying distribution of features in its input dataset and, thus, recognize anomalous data through its inability to reconstruct such events with low error.

VAEs extend this concept to perform Bayesian inference via a latent space that can accommodate a distribution of encoded information. The VRNN architecture combines the variational inference capabilities of a VAE with the sequence modeling provided by an RNN. The inclusion of a learned, time-dependent prior distribution is an essential feature of the VRNN and allows the modeling of complex structured sequences with high variability.

The VRNN is trained on large-R TCC jets in the ATLAS Run 2 dataset satisfying the criteria in Sec. VI for full trigger efficiency, the jet requirements described in Sec. IV, and $p_T(J) > 1.2$ TeV. Its architecture is the same as

that described in Ref. [39]. Training is performed using the PyTorch deep-learning library [47], and the network is updated using the Adam optimizer [48] with a learning rate parameter of 10^{-5}. No regularization via weight decay is applied, but gradient clipping is used with a clip value of 10.

The input jets are modeled as a sequence of up to 20 constituent four-vectors per jet, ordered in k_t splitting starting from the highest-p_T constituent. The p_T selection is designed to chose input jets with highly boosted topologies, for which the VRNN is expected to most improve the sensitivity over the substructure-based approach, as these topologies are well described by k_t-sorted sequence modeling and are also challenging to distinguish with substructure methods. The training is conditioned on four high-level variables, namely the energy-correlator substructure variable D_2 [49,50] for two-prong sensitivity, the N-subjettiness ratio τ_{32} [51] for three-prong sensitivity, and the two k_t-splitting-scale ratios d_{12} and d_{23} [52]. An alignment procedure applied to each jet rescales to the same p_T, boosts to the same energy, and rotates to the same orientation in η and ϕ, inhibiting the VRNN from selecting jets with rare kinematic properties without considering internal constituent structure. This input modeling is designed to reveal correlations between constituents and substructure, allowing the VRNN to distinguish jets with anomalous energy-deposition patterns from the background of homogenous jets originating from QCD processes.

Since the input consists solely of jets from data, no labeling scheme is used in training, distinguishing this method of unsupervised learning from traditional supervised machine learning, where the input is labeled in signal or background categories. Of the data meeting the above criteria, 90% is used for training and 10% for validation. No blinding criterion is applied to the training data, so events that are used in training may also enter the final analysis regions. Since the VRNN performance is consistent across a variety of signal contamination fractions in training [39], and the presence of signal in the training dataset would only lower the sensitivity and cannot produce a false excess, biasing the final result is not a concern.

The loss function of the VRNN is composed of two terms: a reconstruction error term, to minimize differences between the decoded result and the original input, and the Kullback-Leibler (KL) divergence D_{KL} [53] of the encoded approximate posterior distribution from the Gaussian prior distribution. The loss $\mathcal{L}(t)$ for each time step t is given by Eq. (1), where $\mathbf{x}(t)$ is the input constituent four-vector, $\mathbf{y}(t)$ is the output constituent four-vector, z is the approximate posterior, z_t is the learned prior, and λ is a constant parameter to weight the D_{KL} contribution:

$$\mathcal{L}(t) = |\mathbf{y}(t) - \mathbf{x}(t)|^2 + \lambda D_{KL}(z\|z_t). \qquad (1)$$

Here, the time step of the RNN refers to the location in the input sequence. The learned prior z_t is a function of the current time step's hidden state, and the hidden state is updated via a recurrence relation after each time step. An overall loss $\mathcal{L}$ over the sequence is then computed by averaging the individual time-step losses over the length of the sequence.

The KL divergence of the encoded posterior distribution from the true posterior distribution is jointly minimized along with the loss $\mathcal{L}(t)$, ensuring that the architecture accurately describes the underlying distribution of data [54]. The D_{KL} term has been shown to provide better discrimination between anomalous and standard jets than either the reconstruction error or the loss term as a whole. The anomaly score is therefore defined in terms of the D_{KL} of each constituent, averaged over the whole jet, and restricted to the range of $(0,1)$ via exponentiation, as shown in Eq. (2). The resulting variable S_A ensures that more-anomalous jets populate higher values and background populates lower values and is defined as

$$S_A = 1 - e^{-D_{KL}}. \qquad (2)$$

The performance of the VRNN can be assessed by applying Eq. (2) to both background and a variety of signal models and studying the discrimination power of S_A. Its performance in this analysis and the use of the anomaly score to select the X jet are described in the following section.

VI. EVENT SELECTION

The experimental signature of the $Y \to XH$ signal contains at least two jets with high transverse momentum. Signal-like events are selected through event-level criteria, along with jet-tagging criteria for both the X and H boson. In total, the analysis is performed three times, once for each of the three signal regions (SRs). The three analysis categories are defined using the selection criteria for the X particle. Each signal region utilizes five background estimation regions, composed of three control regions (CRs) and two validation regions (VRs), which are defined using common selections on the Higgs boson. The definitions of these regions and motivation for the selection criteria are provided in this section.

The analysis uses data events passing a high-p_T-threshold single large-R-jet trigger. Selected events must have a primary vertex and at least two large-R jets. Only the two highest-p_T large-R jets in an event are considered further, and at least one of their masses must exceed 50 GeV to remove poorly reconstructed events. To ensure that the trigger is fully efficient, the invariant mass of the two large-R jets must satisfy $m_{JJ} > 1.3$ TeV and the leading large-R jet, J_1, must have $p_T(J_1) > 500$ GeV. These requirements, along with a selection on the $D_{H_{bb}}$ score defined in the next subsection, compose the analysis preselection.
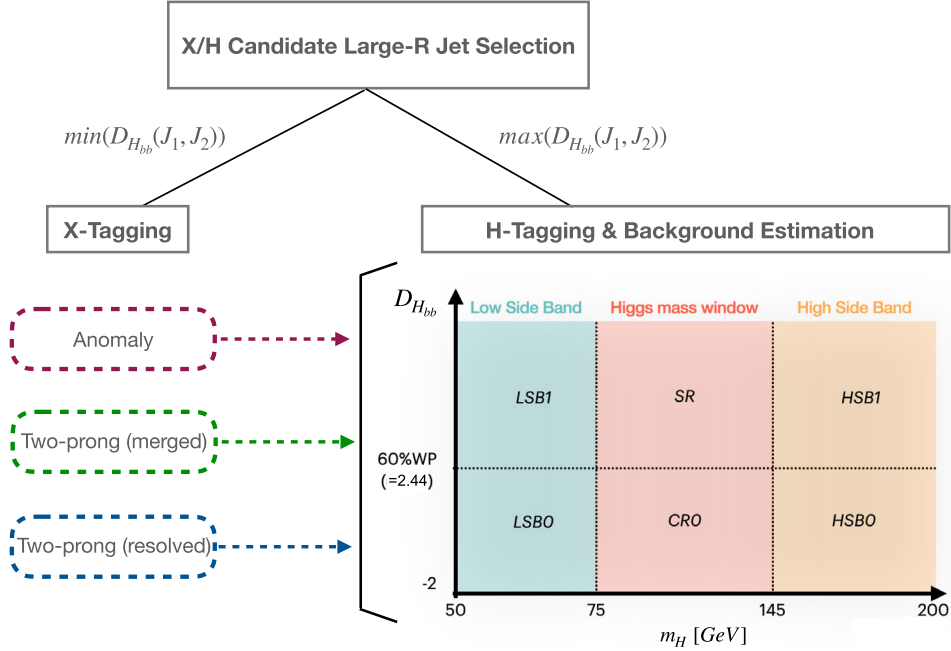
FIG. 2.   Illustration of the selection flow, after preselection, and the analysis regions of the $Y \rightarrow XH$ search. The first step in resolving the ambiguity in assigning the two large-R jets to X and H candidates dictates which jet is used to make the first selection on either D_2^{trk} or the anomaly score of the X candidate. This sorts the preselection events into three separate categories, namely anomaly, two-prong merged, and two-prong resolved. Each region has its own background estimation and validation regions. The CRs (CR0, HSB0, HSB1), VRs (LSB0, LSB1), and SR are defined in the same way for all three analyses using the H candidate mass (m_H) and $D_{H_{bb}}$ score. The large-R jet J_H is required to have $D_{H_{bb}} > -2$.

As mentioned previously, the three analysis SRs vary in the selection criteria for the X particle. The primary SR, using the VRNN for generic X tagging, is referred to as the *anomaly SR*. The other two SRs target the benchmark $X \rightarrow q\bar{q}$ decay and are thus called the *two-prong SRs*. Here the jet substructure is used to distinguish reconstruction of the X particle as either a single large-R jet (*merged SR*) or two small-R jets (*resolved SR*). They are not required to be orthogonal to the anomaly SR but do not overlap with each other. The analysis CRs include the high sideband (HSB) of the Higgs boson candidate mass m_H, used to generate the DNN reweighting for the background estimation procedure, and CR0, which provides the final background template for the SR. The VRs are defined in the low sideband (LSB) of the Higgs boson candidate mass and validate the reweighting derived from the HSBs. The full analysis flow is shown in Fig. 2, with selection details provided below.

A. X/H ambiguity resolution

Since the SRs are constructed by placing requirements on the different properties of the X and H large-R jets, an ambiguity must be resolved to determine which of the two J's in the event is more likely to be the Higgs boson and thus subject to the Higgs boson selection criteria. This is done by using a classifier based on a neural network (NN) to separate bosons decaying into $b\bar{b}$ from top-quark and

QCD jets [55]. The tagger is trained on the large-R jet p_T and η, along with the subjet flavor-tagging score DL1r [56] for up to three track subjets constructed with a jet-p_T-dependent radius parameter [57]. The tagger version used here includes a reweighting of all training inputs to have the same p_T and η distributions, to minimize biasing of the tagger toward high-p_T or central jets, respectively. The outputs of the NN are three classification scores corresponding to the probability for the jet to have originated from a Higgs boson (P_{Higgs}), top quark (P_{top}), or multijet process (P_{multijet}), and these are subsequently combined into the jet-level discriminant $D_{H_{bb}}$:

$$D_{H_{bb}} = \ln \frac{P_{\text{Higgs}}}{f_{\text{top}} \cdot P_{\text{top}} + (1 - f_{\text{top}}) \cdot P_{\text{multijet}}}. \quad (3)$$

In Eq. (3), f_{top} determines the weight assigned to the top-quark background shape in the final discriminant, and its chosen value of 0.25 is based on signal-to-noise optimization studies.

To perform the large-R jet ambiguity resolution, $D_{H_{bb}}$ is computed for both J's in the event. The jet with the larger value of $D_{H_{bb}}$ is labeled as the Higgs boson candidate (J_H), and the other J is by default the X candidate (J_X), thus determining which jet is subject to further H and X selection. This procedure has an accuracy of over 90% in the highly boosted region of the signal grid
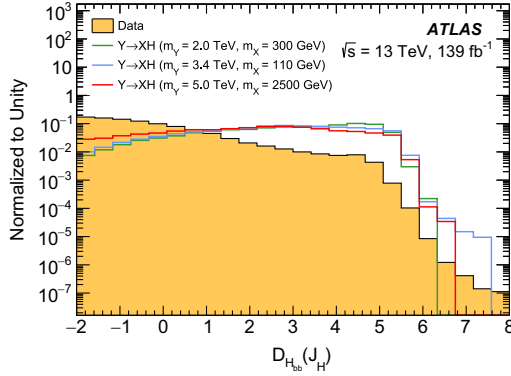
FIG. 3. Distributions of the J_H candidate $D_{H_{bb}}$ score in data after preselection requirements are applied. Also shown are three $Y \to XH$ simulated signals, labeled by the masses of the Y and X particles. Requiring $D_{H_{bb}} > 2.44$ defines a working point that is 60% efficient for the selection of the boosted $H \to b\bar{b}$ topology across the full p_T range. All distributions are normalized to unity.

$(m_X/m_Y < 0.5)$, decreasing to no less than 75% for less boosted mass points where the boosted $H \to b\bar{b}$ tagging is less efficient. The resulting distribution of $D_{H_{bb}}$ for the J chosen as the Higgs boson candidate, for both data and representative $Y \to XH$ signals at preselection, is shown in Fig. 3. Additionally, a preselection of $D_{H_{bb}} > -2$ is applied to remove events that are determined to be not $H \to b\bar{b}$-like, thus ensuring the data-driven background estimation focuses on a phase-space region that is close to that of the signal.

B. X selection

After the X candidate's J is determined, a region-dependent selection is applied to enhance the anomalous-jet content in the anomaly, two-prong merged, and two-prong resolved regions. The anomaly region is defined using the anomaly score value S_A of the X jet as determined by the VRNN. Figure 4 shows the resulting distribution of

X candidate S_A values after the analysis preselection is applied, comparing data with three different $Y \to XH$ baseline signal samples as well as the three signals with alternative X decays. The absence of signal information in the construction of the score means that it is not expected to outperform analytic or supervised methods for any single signal model. However, using the VRNN approach to characterize the background distribution provides broad sensitivity to a variety of signals that differ from jets originating from QCD processes. The most notable difference in S_A shape is found for dark jets, which have a substructure that is not well characterized by existing variables. The dependence of the sensitivity on kinematics is also relevant to performance, as the S_A distribution for the highly resolved point ($m_Y = 5000$ GeV, $m_X = 2500$ GeV) populates lower, and thus less anomalous, values than the data, making this signal indistinguishable from background in the anomaly detection approach. A selection $S_A > 0.5$ is chosen for the J_X candidate and provides modest but comparable discrimination power in data for the disparate signal-jet topologies considered in the full expected p_T range of the X candidate jets. This enhances the signal-to-background ratio for the two boosted points, ($m_Y = 2000$ GeV, $m_X = 300$ GeV) and ($m_Y = 3400$ GeV, $m_X = 110$ GeV), by approximately 25% relative to the inclusive selection.

Regions focusing on the benchmark $X \to q\bar{q}$ decay are used to supplement the anomaly detection analysis and interpret the results. The merged region is defined by applying a selection $D_2^{\text{trk}} < 1.2$, where D_2^{trk} is the same as D_2 but computed using only tracks associated with the jet. The choice of using only tracks in the D_2 calculation is motivated by the ability to propagate track-only uncertainties into the final signal efficiency. Detailed comparisons of D_2^{trk} with the standard D_2 variable at analysis preselection have shown D_2^{trk} and D_2 to be highly compatible, ensuring its sensitivity to two-prong signals with respect to multijet background. Because jets with
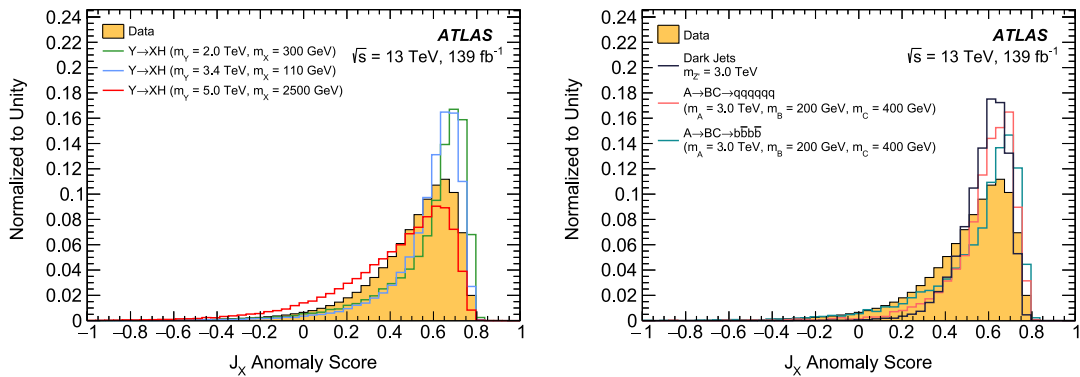

FIG. 4. Distributions of the J_X candidate anomaly score (S_A) in data after preselection requirements are applied. Also shown are three $Y \to XH$ simulated signals (left), labeled by the masses of the Y and X particles, and the three additional signals with alternative X decay hypotheses, namely heavy-flavor, three-prong, and dark jet (right). A selection $S_A > 0.5$ applied to J_X defines the anomaly analysis category. All distributions are normalized to unity.
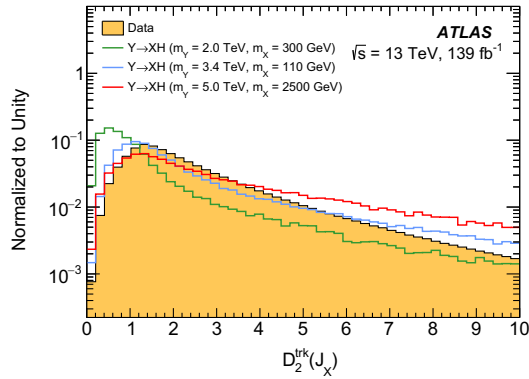
FIG. 5. Distributions of J_X candidate D_2^{trk} in data after preselection requirements are applied. Also shown are three $Y \to XH$ simulated signals, labeled by the masses of the Y and X particles. A value of $D_2^{\text{trk}} = 1.2$ therefore separates the analysis events into merged (< 1.2) and resolved (> 1.2) two-prong categories. All distributions are normalized to unity.

two-prong substructure have lower values of D_2^{trk}, this selection enhances the presence of fully merged decays where the X decay products are well contained by a single J. Since the efficiency of substructure variables is mainly driven by the boost of the large-R jet and therefore its p_T, the optimal cut value of 1.2 was chosen so as to maximize signal-versus-background discrimination across the p_T range of the X candidate, combining all mass points in the $Y \to XH$ grid. Distributions of D_2^{trk} for J_X are shown in Fig. 5 for both data and representative $Y \to XH$ signals at preselection.

Due to kinematic constraints driven by the m_X/m_Y ratio, events that fail the merged selection typically also show poor reconstruction of the X mass by the large-R jet. In these events, the large-R jet does not sufficiently contain all of the X decay products, leading to an underestimation of the X particle mass. To achieve better sensitivity in this regime, a resolved selection is defined by requiring the D_2^{trk} value of J_X to be greater than 1.2, corresponding to a less boosted X particle which is more appropriately reconstructed using two small-R jets. A dedicated algorithm matches two small-R jets to the X by requiring at least four j in the event, discarding the two with the smallest ΔR to the Higgs boson candidate J_H, and selecting the two remaining small-R jets with the highest p_T. The mass of the Y resonance is then computed using the Higgs boson candidate large-R jet and the two small-R jets matched to the X. Additional requirements of $|\Delta y_{j1,j2}| < 2.5$ and a p_T imbalance $p_T^{\text{bal}} < 0.8$ are applied to aid accurate resolved X reconstruction; here Δy refers to separation in rapidity and p_T^{bal} is defined as the difference of the X particle's small-R jet transverse momenta divided by their sum. The resolved region improves the signal efficiency for points with higher m_X/m_Y (corresponding to less boost for the X candidate

decay) by a factor of approximately 5 relative to the boosted selection.

C. H selection

The Higgs boson tagging is performed after the J_X selection is applied and sorts the events into the three analysis categories, for which the background is estimated. For all signal regions, a requirement $D_{H_{bb}} > 2.44$ providing a constant 60% efficiency across jet p_T is applied to the Higgs boson candidate J_H, along with a mass window requirement of $75 < m_H < 145$ GeV. The data-driven background estimation uses events from the HSB of the Higgs boson candidate mass ($145 < m_H < 200$ GeV), which are further separated into HSB0 and HSB1 depending on whether the Higgs boson candidate J_H fails or passes the $D_{H_{bb}}$ selection. Validation is performed in the LSB, where the reconstructed Higgs boson mass must be between 65 and 75 GeV. LSB0 and LSB1 are similarly defined as having Higgs boson candidates that fail or pass the $D_{H_{bb}}$ tagging criterion, respectively. CR0 is defined as the set of events where the H boson is in the SR mass window but fails the $D_{H_{bb}}$ tagging. DNN-based reweighting is applied to CR0 to obtain the final background prediction in the SR. The contamination from signal events is found to be of the order of a few percent in the HSB and no more than 10% in the LSB, for all mass points in the $Y \to XH$ grid.

In total, three SRs and 15 background estimation regions, five for each SR, are used in the analysis. A summary of all region definitions is provided in Table I.

D. Binning optimization

The signal search in the two-dimensional space of m_Y versus m_X applies a variable-width sliding window to the J_X candidate mass spectrum, dividing the data into a series of overlapping m_X ranges in which the m_{jj} distribution is fitted. The chosen binning for m_Y and m_X is based on the ATLAS detector's mass resolution for a generic narrow-width resonance, given by the fitted width of the Gaussian core of a double-sided Crystal Ball function. Modifications are made to the binning to account for the limited number of data events. In the m_Y spectrum, bins are widened at higher values of m_Y to ensure that at least one event is present in each bin when using LSB1 data. For the m_X categories, an initial set of mass windows is generated from a linear fit of m_X resolution as a function of m_X. The first window is chosen to have a bin center at $m_X = 65$ GeV, the lowest generated signal X mass, and its width is chosen to be twice the resolution obtained from the fit. Subsequent windows, increasing in m_X, are chosen in the same way, where their bin centers are selected to be higher than the previous window's bin center by an amount that is equivalent to half of the previous window's mass resolution. The widths of high-mass windows are expanded

TABLE I. Preselection requirements and optimized requirements defining the SRs and background estimation regions.

Parameter	Preselection requirements
m_{jj} [GeV]	>1300
$p_T(J_1)$ [GeV]	>500
m_J [GeV]	$m_{J_1} > 50 \| m_{J_2} > 50$
$D_{H_{bb}}$	> -2

	Signal regions		
	Merged	Resolved	Anomaly
m_H [GeV]	(75, 145)	(75, 145)	(75, 145)
$D_{H_{bb}}$	>2.44	>2.44	>2.44
D_2^{trk}	<1.2	>1.2	…
$\|\Delta y_{j_1,j_2}\|$	…	<2.5	…
p_T^{bal}	…	<0.8	…
Anomaly score (S_A)	…	…	>0.5

	Background estimation regions				
	CR0	HSB0	HSB1	LSB0	LSB1
m_H [GeV]	(75, 145)	(145, 200)		(65, 75)	
$D_{H_{bb}}$	<2.44	<2.44	>2.44	<2.44	>2.44

symmetrically, based on event counts in LSB1, until at least ten events are present in each final m_X bin. In order to avoid having duplicate windows, all resulting windows which share at least one bin edge are replaced by a single window encompassing their union. Finally, to accommodate the highest signal mass point at $m_X = 3000$ GeV, the last bin's upper edge is placed at 3200 GeV.

VII. BACKGROUND ESTIMATION

The expected SM background that contributes in the SRs arises mainly from high-p_T multijet events, with jets that imitate the $b\bar{b}$ or X topologies. Simulation of such QCD processes is known to suffer from mismodeling and is computationally expensive. Therefore, in this analysis the background estimation is fully data-driven and uses regions that are orthogonal to the SR because of their Higgs boson jet criteria.

The shape of the expected m_{jj} distribution in the SR is obtained from data in CR0, and weights are derived that can be applied to HSB0 to reproduce the shape found in HSB1. This procedure is validated by applying the weights to data in LSB0 and comparing the resulting m_{jj} spectrum with that observed in LSB1 data. The weights are generated inclusively in the X candidate selection and applied separately to create three background predictions, one for each SR.

The reweighting function is defined as the ratio of the multidimensional probability distribution function of data in HSB1 to that of data in HSB0. In this analysis, the statistical procedure of *direct importance estimation* [58,59] is utilized, where the ratio is estimated directly from data without having to analytically compute each individual PDF. It is implemented via the training of a DNN, where a custom square-root loss function [60] is chosen to produce weights that can accurately reproduce the observed ratio in data. The DNN outputs event-level weights that are assumed to be approximately independent of m_H, an assumption that can be verified using events in the LSB, and thus can be applied to an untagged region to produce the m_{jj} shape in the corresponding $H \to b\bar{b}$-tagged region.

Events are considered for training the DNN if they pass the analysis preselection, satisfy $145 < m_H < 175$ GeV, and additionally have at least two track jets associated with the Higgs boson candidate J. They are modeled as a set of variables, namely the transverse momentum, pseudorapidity, azimuthal angle ϕ and energy of the Higgs boson candidate; the number of tracks associated with the Higgs boson candidate; and the transverse momentum, pseudorapidity, ϕ and mass of the first two track jets associated with the Higgs boson candidate, ordered in p_T. Each variable x is standardized with the transformation $x = (x - \mu)/\sigma$, where μ and σ are the mean and the standard deviation of the distribution of the x variable.

The DNN is built using a fully connected sequential model from Keras [61] with three inner layers, each with 20 neurons and a rectified linear unit activation function. In order to reduce the problem of overfitting during training, 10% of connections among inner layers are randomly severed (called "dropout"). The last layer has a single output with a simple linear activation function. The model is trained using the Adam optimizer [48] in Keras, with TensorFlow [62] as its back end. Training is performed using a batch size equal to the full dataset size for 1600 epochs, with early stopping at 100 epochs if the value of the loss calculated on the validation dataset does not decrease for 100 subsequent epochs.

The output weights of the DNN are validated using data in the LSB. Figure 6 shows the impact of the reweighting on distributions of several key analysis variables, using the two-prong merged LSB VR as an example. Three curves are shown for each variable, comparing the LSB0 data, before and after DNN reweighting is applied, with the target data distribution in LSB1. These variables are chosen so as to focus on kinematic variables of the Higgs boson, whose properties are used to distinguish the CR from the SR, and variables involved in the final statistical treatment. Good agreement between the reweighted shape and the true tagged data is observed for each variable, suggesting a robust background model. Since the training is performed
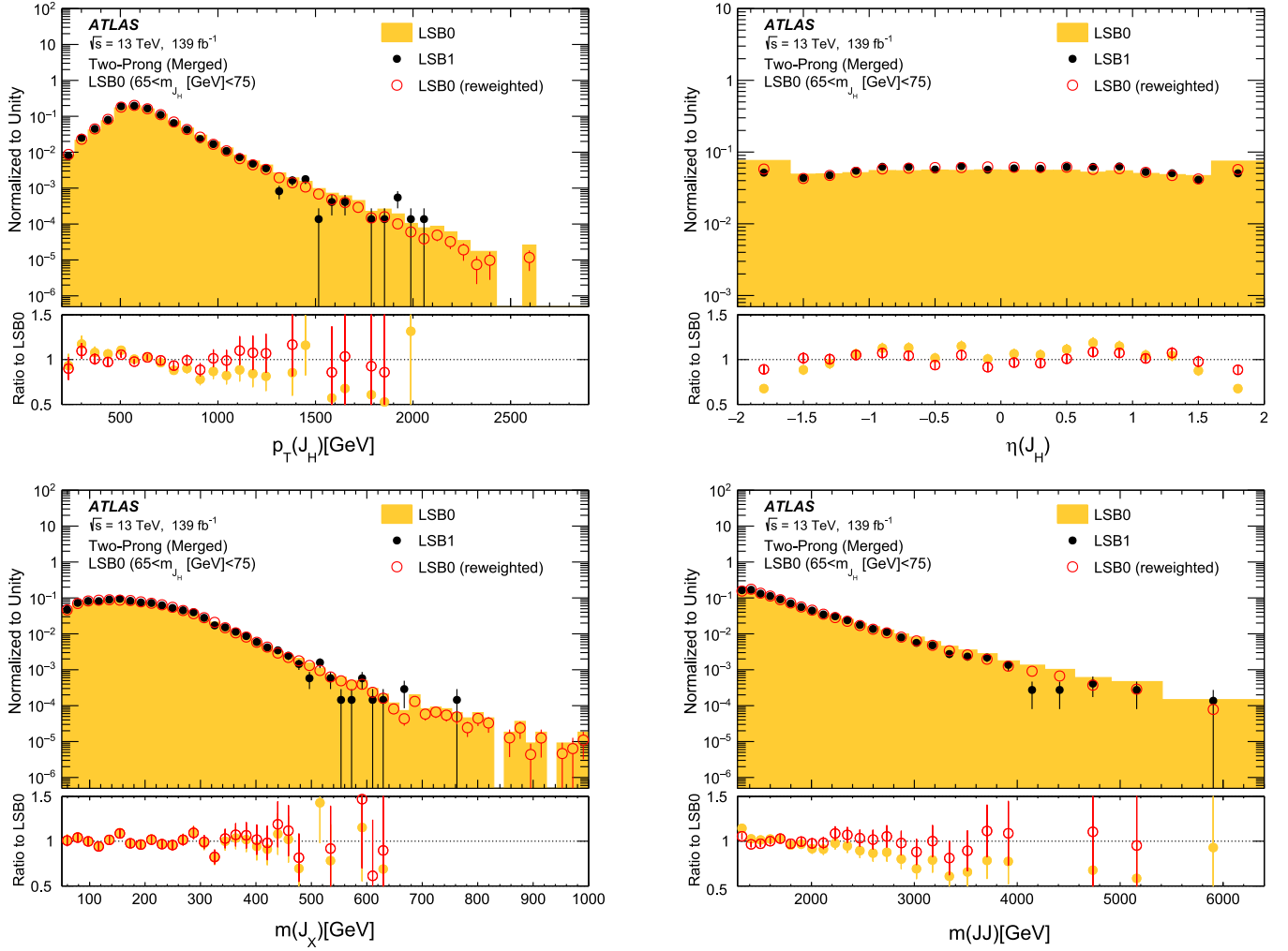
FIG. 6. Distribution of (a) p_T and (b) η for the H candidate J, along with (c) the mass of J_X and (d) m_{jj} in the merged LSB validation region, overlaying data from LSB1 (solid black points) with the data in LSB0 shown before (orange histogram) and after (red circles) reweighting. The ratio of the LSB1 data to both the LSB0 data (orange) and the reweighted LSB0 data (red) is shown in the lower panel. Error bars indicate statistical uncertainties.

inclusively in the X tagging, the same conclusion holds for the anomaly and two-prong resolved LSB regions, which is verified in comparisons of distributions between the reweighted LSB0 and LSB1 in those regions. Also, since the reweighting is applied to m_{jj} distributions after the X-tagging selection is applied, no extrapolation across D_2^{trk} or S_A is required, and the method shows similar background modeling across all three SRs. Any minor residual differences between predicted background and data in the SRs are covered by the nonclosure systematic uncertainty, described in Sec. VIII.

VIII. SYSTEMATIC UNCERTAINTIES

Systematic uncertainties affect both the data-driven background estimate and the simulated signal. All background uncertainties are estimated using an m_{jj} shape that is inclusive in m_X and applied to each m_X category fully correlated among m_{jj} bins. Background shape variations are derived from three sources.

The first is from training the DNN in an alternative region of $165 < m_H < 200$ GeV to account for the way in which phase-space uncertainties may affect the obtained weights. This region has approximately the same number of events and tagging efficiency as the nominal training region, helping to isolate the way in which changing only the DNN model affects the weights. Upward and downward variations are defined by symmetrizing the shape difference in m_{jj} between the two different models, yielding an effect of $\mathcal{O}(1\text{--}10)\%$ across the distribution.

Another DNN variation accounts for the finite size of the training sample and the random initialization of the weights. It is estimated with a bootstrap procedure [63,64] where a set of 100 bootstrap networks are trained. For each training, the training dataset is varied by resampling it with replacement, assigning to each event a new weight

that comes from a Poisson variable with a mean of one. Two additional templates are formed to create a symmetric error band by taking the median weight for each event and adding or subtracting half of the interquartile range. This corresponds to a $\mathcal{O}(1)\%$ effect across m_Y.

Lastly, a nonclosure uncertainty is included to cover modeling discrepancies that may arise when weights derived from the NN training in the HSB are extrapolated to the LSB and subsequently to the SR. It is defined by the symmetrized shape difference between the data and predicted background in the LSB. To avoid being sensitive to statistical fluctuations in the LSB, smoothing is applied to the variation, where it is rebinned to reduce the relative statistical uncertainty. The nonclosure uncertainty is negligible for low m_{jj} and rises to $\mathcal{O}(10)\%$ in the m_{jj} tails.

Normalization and shape uncertainties are applied to the simulated signals. An uncertainty of 1.7% is applied to the luminosity measured with the LUCID-2 detector [65]. The uncertainty from the trigger selection is negligible, and thus not included, since the requirement of $m_{jj} > 1.3$ TeV ensures that the trigger is fully efficient.

Scale factors (SFs) computed to match the $H \to b\bar{b}$ tagger efficiency between data and simulation are applied to the signal template, and their uncertainties are similarly propagated to the signal normalization. These SFs are computed using the methodology described in Ref. [66], with the substitution of an updated $D_{H_{bb}}$ that includes the η reweighting of inputs as described in Sec. VI. They are binned in large-R-jet p_T, where the SF for the highest p_T bin is extrapolated to cover the upper end of the p_T region probed by the analysis selection. Agreement between data and MC simulation for these SFs is verified with $Z \to b\bar{b}$ events in calibration studies. The SFs are bounded by approximately 1.1 and 1.4 across all p_T bins, with uncertainties in the range of approximately $\pm(0.3$–$0.5)$.

Instrumental systematic uncertainties arise from uncertainty in the jet p_T scale and resolution, for both the large-R and small-R jets, and affect the shape of the m_{jj} distribution. Uncertainty in the large-R-jet p_T scale is an important effect in the search for resonant structures in the presence of rapidly falling background spectra, as it can shift the peak of the resonance. It is evaluated using tracking-to-calorimetric p_T double ratios between data and simulation, where any observed differences are assigned as baseline systematic uncertainties [67]. Even though the analysis relies on jets built from TCCs, the total p_T of the jet is still solely derived from calorimeter information, keeping it independent of the track-based jet p_T. Past analyses have studied the possible impact of calorimeter versus track-based p_T by cross-calibrating between per-jet TCC and calorimeter p_T and found it to be negligible [30]. The total jet-p_T-scale uncertainty varies with p_T and η and is typically around $\pm 5\%$. Uncertainties from the reconstruction and modeling of tracks are also taken into account; these cover track reconstruction efficiency, impact parameter resolution,

tracking in dense environments, fake-track rates, and sagitta biases. The impact of the large-R-jet p_T resolution uncertainty is evaluated event by event by rerunning the analysis with an additional absolute 2% Gaussian smearing applied to the input jets' p_T to degrade the nominal resolution. Small-R-jet p_T scale and resolution uncertainties are similarly estimated by comparing data with simulation after applying *in situ* corrections [68].

Several sources of theoretical uncertainty affecting the signal models were considered. Uncertainties in the matrix element calculation are evaluated by varying the strong coupling constant (α_s), the renormalization scale (μ_r), and the factorization scale (μ_f). The effects of uncertainties in the parton distribution functions are evaluated by comparing the m_{jj} distributions obtained when using various alternative PDF sets and taking an envelope of these distributions, as prescribed by the PDF4LHC group [69]. Generator-level variations of the A14 tune's parameter values are used to cover the initial- and final-state radiation (ISR and FSR, respectively) and multiple parton interaction (MPI) uncertainties. An overall conservative 3% normalization uncertainty is applied to all signals as a result of ISR, FSR, and MPI modeling effects.

IX. STATISTICAL ANALYSIS

The statistical framework in the analysis is used to perform hypothesis tests in the SRs, testing the compatibility of the data with both the background-only and signal-plus-background hypotheses. The observable that is fitted is the m_Y distribution of the data in the SR. This fit is repeated several times in overlapping bins of the X candidate mass.

The parameter of interest in the statistical analysis is the signal strength μ, defined as a scale factor multiplying the nominal yield predicted by a 1 pb signal cross section so as to match the observed number of signal events. The background-only hypothesis corresponds to $\mu = 0$. The normalization of the data-driven background estimate is allowed to float, with each normalization factor being fitted independently because the m_X categories overlap. A test statistic based on the profile likelihood ratio calculated in the lowest-order asymptotic approximation is used to test the models corresponding to the signal grid. Systematic uncertainties are included in the fit as nuisance parameters (NPs) with Gaussian constraints. Both the signal strength and all signal systematic uncertainty NPs are correlated across the merged and resolved regions. The significance of an observed excess of data over the background prediction is quantified by the local p value, which is the probability that the background-only model produces an excess at least as large as the one observed.

BumpHunter [70] is used to find excesses in both the anomaly and two-prong SRs, with an algorithm that incorporates only the statistical uncertainty of the data and does not depend on a specific signal shape. It outputs a
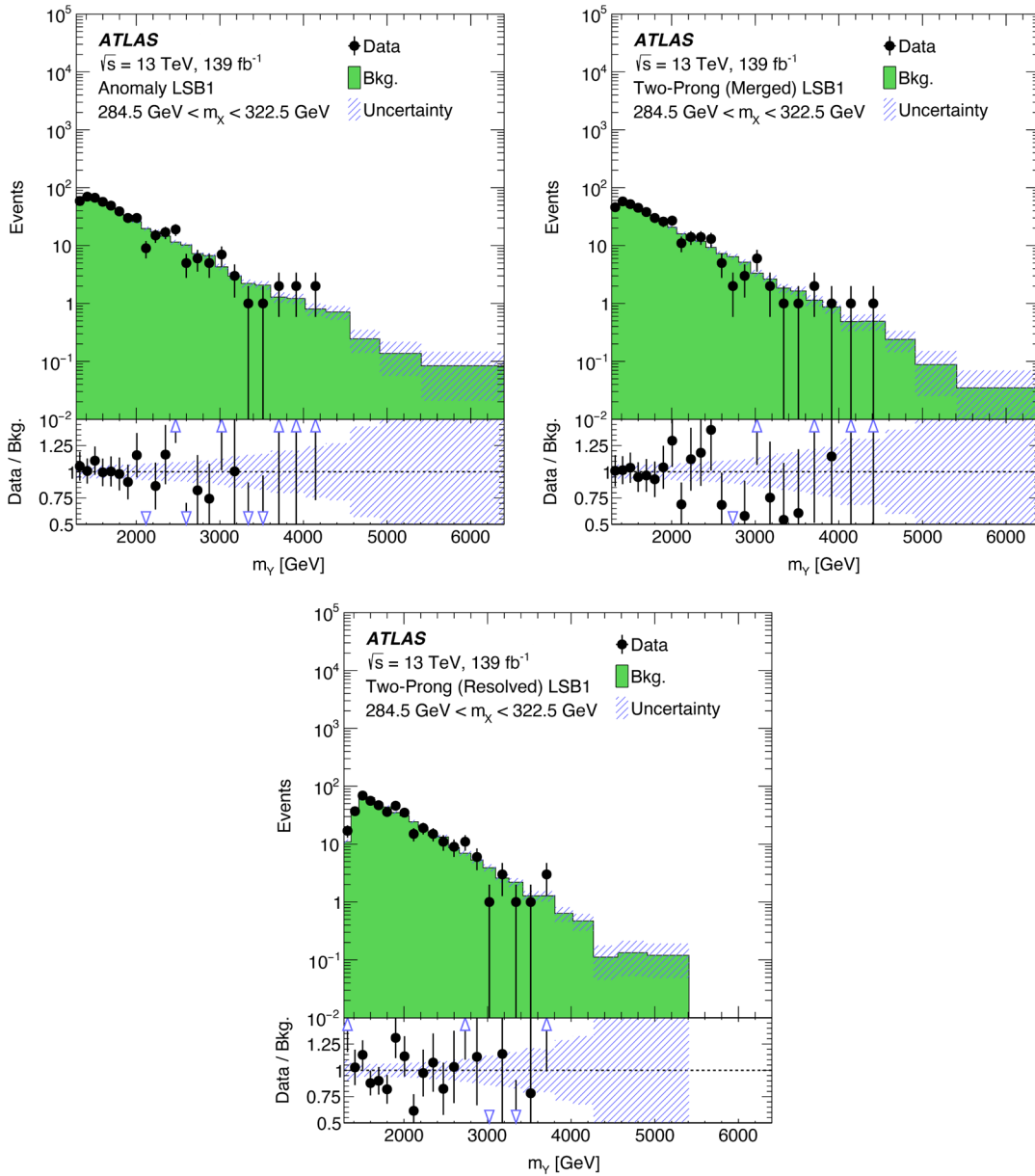
FIG. 7. Reconstructed m_Y distributions of the background, as determined by a background-only fit, and data in the LSB1 VR, for the anomaly, two-prong merged, and two-prong resolved selections, in the m_X bin [284.5, 322.5] GeV. The ratio of the observed data to the background is shown in the lower panel. The uncertainty band includes both the statistical and systematic effects.

p value that provides a goodness-of-fit metric, along with an interval of the invariant mass corresponding to the largest deviation of the data from the background prediction. It is thus used in all signal regions to search for significant deviations of the data from the background m_Y distribution. Dedicated studies indicate the fits are dominated by statistical uncertainties, further motivating the discounting of systematic uncertainties in the BumpHunter fits. In the anomaly SR, no subsequent fits are performed using the $Y \rightarrow XH$ signal model, as this analysis is designed to keep signal-model dependence minimal and the two-prong regions are expected to have higher signal sensitivity across the $Y \rightarrow XH$ grid. However, given the

absence of a significant excess in the two-prong regions, signal-plus-background fits are performed for each $Y \rightarrow XH$ signal model, and 95% confidence level (CL) upper limits on the signal cross section are set using a modified frequentist method (CL$_s$) [71].

The background estimation and statistical treatment are validated by comparison with data in the signal-depleted LSB VR for each of the three analysis categories. BumpHunter p values from all m_X-bin fits in the VR of the anomaly region approximate a flat distribution between 0 and 1, indicating good background modeling with no systematic biases across the phase space. Figure 7 shows the postfit background prediction compared with the data
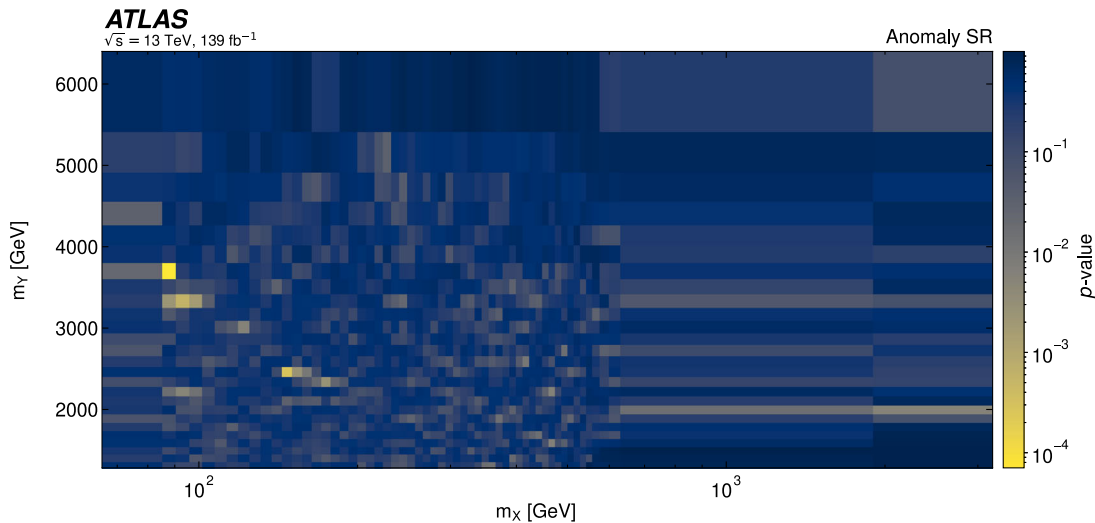
FIG. 8. The distribution of observed p values across all m_Y and m_X bins in the anomaly signal region, comparing data with the background estimates generated by a background-only fit, displayed in the two-dimensional (m_X, m_Y) grid. The p-value calculation is performed at the center of each m_X bin, and all statistical and background systematic uncertainties are considered. The lowest observed p value corresponds to the bin with m_Y within $[3608, 3805]$ GeV and m_X within $[75.5, 95.5]$ GeV.

passing the anomaly, merged, and resolved selections, in an example m_X window between 284.5 and 322.5 GeV where the whole kinematic phase space is well populated. Good modeling is observed, and no significant pulls or constraints are observed in the background NPs. In the two-prong regions, checks are made for spurious signals in the LSB through a signal-plus-background fit using each generated signal model. These checks indicate that no significant spurious signal is present beyond those likely to be produced by statistical fluctuations, with no systematic trend across the expected phase space.

X. RESULTS

Results of background-only fits of the m_Y distribution across all m_X categories in the anomaly SR show the data to be compatible with the expected backgrounds given their uncertainties. Figure 8 shows the distribution of p values across m_Y and m_X bins, where the background is the result of a background-only fit performed with all statistical and systematic uncertainties, and all uncertainties are included in the p-value calculation. The distribution of observed p values is statistically compatible with the expectation, with a χ-squared value per degree of freedom of 1.32 between the distributions.

The largest observed excess in the anomaly SR is in the m_X window $[75.5, 95.5]$ GeV. In this window, the greatest single-bin excess is found for m_Y between 3608 and 3805 GeV. The BumpHunter interval with the greatest significance covers the m_Y range between bin edges of 3424 and 3805 GeV. The m_Y distribution corresponding to this m_X window is shown in Fig. 9, along with the postfit expected background. Studies of the individual jet mass distributions in this m_X category do not reveal any excesses

in data that are consistent with a resonant particle decay. Given the number of individual search regions in this analysis, the impact of the trials factor is significant. A calculation is made to determine the global significance of the greatest single-bin deviation, accounting for all the
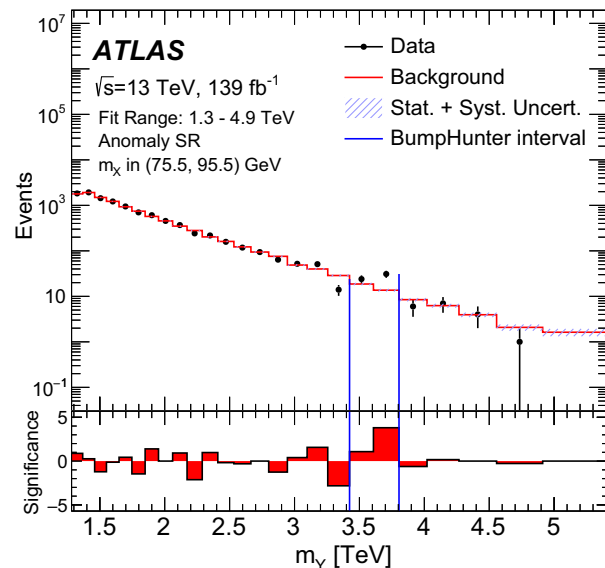

FIG. 9. The m_Y distribution associated with the m_X bin $[75.5, 95.5]$ GeV in the anomaly SR, where the background is determined by a background-only fit to data with both the statistical and systematic uncertainties included. The p value and the lower panel of per-bin significances are computed with statistical uncertainties only. The single m_Y bin with the most significant excess is $[3608, 3805]$ GeV. Incorporating the trials factor for all m_Y and overlapping m_X bins in the search, this excess has a global significance of 1.43σ.
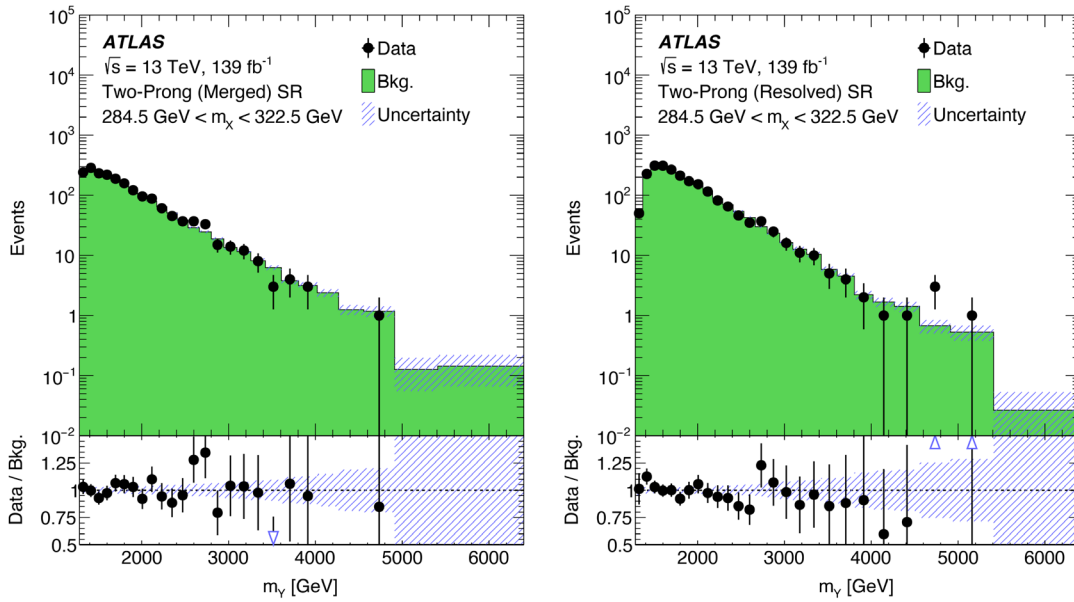
FIG. 10. Reconstructed m_Y distributions of background and data in the SR, for the merged (left) and resolved (right) selections, in the m_X bin [284.5, 322.5] GeV. The background is determined by a background-only fit to the data with all statistical and systematic uncertainties included. The ratio of the observed data to the background is shown in the lower panel. The uncertainty band includes both the statistical and systematic effects.

overlapping m_X bins. First, the overlapping bin edges are used to define exclusive, nonoverlapping bins in m_X, and an integer is drawn from a Poisson distribution with a mean equal to the background expectation in each exclusive (m_Y, m_X) bin. Next, this yield is summed across exclusive bins to create a toy estimate for each overlapping bin in which the p value is computed. Finally, this procedure is repeated N times, where N is the number of events, inclusively across all exclusive, nonoverlapping bins. This calculation yields a global significance of 1.43σ for the excess in the [3608, 3805] GeV bin of m_Y.

Results for the two-prong SRs are similarly derived by performing background-only fits and scanning with BumpHunter for incompatibility with data. No significant deviations of data from the predicted background are observed beyond expected statistical fluctuations, in either the merged or resolved SR. An example m_Y distribution in both the merged and resolved SRs for the m_X bin [284.5, 322.5] GeV is shown in Fig. 10, along with the background estimate that is determined from a background-only fit accounting for all uncertainties. Figure 11 shows a summary of the per-bin p values in each m_Y bin for selected m_X bins that are centered on key X candidate mass hypotheses, namely at the W, Z, and H boson masses.

Given the absence of significant excesses in the data, signal-plus-background fits are performed to determine the 95% CL upper limit on the cross section of the $Y \to XH$ process. A summary of the expected and observed limits in the 2D grid of $Y \to XH$ signals is given in Fig. 12, combining results from the merged and resolved regions.

A bilinear interpolation procedure is applied to provide results between fully simulated signal points. The analysis is most sensitive in the very boosted regime, where the Y mass is approximately an order of magnitude larger than the X mass. Sensitivity is lowest in the highly resolved regime, where the required large-R J reconstruction of the Higgs boson sculpts the signal efficiency to favor high-momentum X particles. The observed limits range from cross sections of 0.341 fb for the signal point ($m_Y = 5000$ GeV, $m_X = 600$ GeV), to 1.22 pb for the signal point ($m_Y = 2500$ GeV, $m_X = 2000$ GeV).

The data in the anomaly and two-prong SRs can be used to provide a benchmark comparison of sensitivity across the set of large-R jet topologies considered for the X decay, thereby providing a metric for assessing the level of signal-model dependence in both regions. The 95% CL upper limits on the production cross section of several benchmark signals are calculated for all three signal region selections, by injecting signal into the data until the BumpHunter p value exceeds a significance of 2σ. Seven signal points are considered in this study, including three highly boosted $Y \to XH$ points, one resolved $Y \to XH$ point, and the three alternative jet topologies. Because the systematic uncertainties in the signal efficiency of the anomaly score are not assessed, this comparison is performed using only statistical uncertainties and a postfit background estimate in the limit calculation.

Since the merged region uses D_2^{trk} and thus explicitly tags on the two-prong substructure of the X candidate's large-R jet in the generated $Y \to XH$ grid, it is possible that this region will outperform the fully unsupervised approach
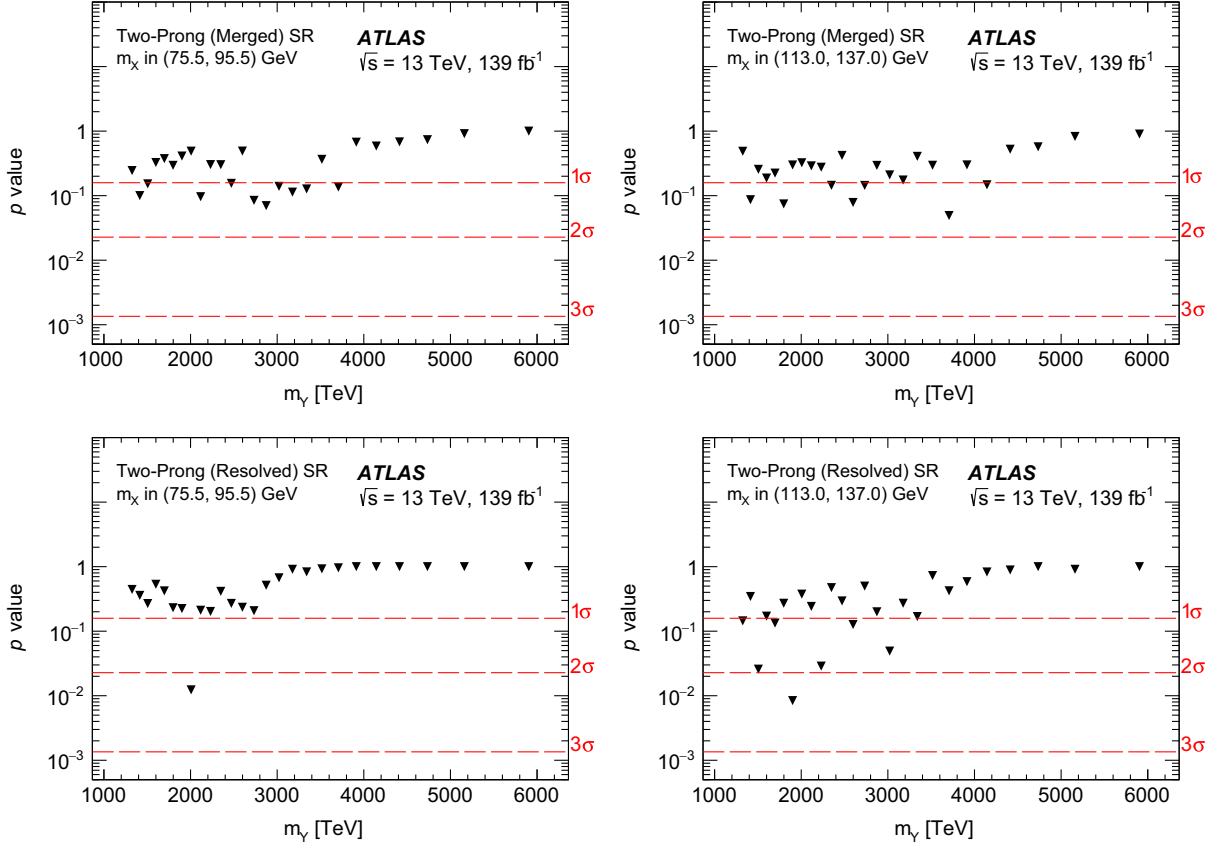
FIG. 11. The p value per m_Y bin for both two-prong SRs, calculated using all systematic and statistical uncertainties of the background estimate. Two m_X bins are shown, [75.5, 95.5] and [113.0, 137.0] GeV, which corresponds to a window containing the W/Z and Higgs boson mass, respectively. Events thus fall in (a) a merged W/Z window, (b) a merged Higgs window, (c) a resolved W/Z window, and (d) a resolved Higgs window. The background is determined by a background-only fit to the data with all statistical and systematic uncertainties included. In both m_X windows, the p value has a high approximately constant value for the high Y-mass region of the resolved SR (bottom), as this phase-space region is far more likely to produce a highly boosted J_X that falls in the merged SR selection.

FIG. 12. The expected (left) and observed (right) 95% CL limits on the cross section $\sigma(pp \to Y \to XH \to q\bar{q}b\bar{b})$ in picobarns in the two-dimensional space of m_Y versus m_X, obtained from a simultaneous fit of both the merged and resolved two-prong signal regions with all statistical and systematic uncertainties. A bilinear interpolation procedure is applied to provide results between fully simulated signal points. The observed limits range from 0.34 fb for the signal point ($m_Y = 5000$ GeV, $m_X = 600$ GeV) to 1.22 pb for the signal point ($m_Y = 2500$ GeV, $m_X = 2000$ GeV). The boundaries of the limit are defined by the simulated signal grid.

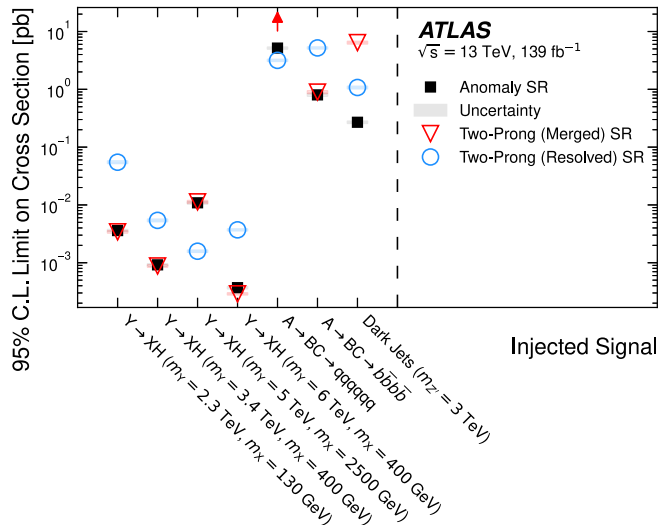FIG. 13. The 95% CL upper limit on the cross section for seven benchmark signal processes, comparing the anomaly, two-prong merged, and two-prong resolved signal region selections. The cross section is obtained by injecting signal into the observed data until 2σ sensitivity is achieved as determined by the BUMPHUNTER interval p value. The background estimate is the result of a fit with all background uncertainties considered, while the BUMP-HUNTER algorithm incorporates only statistical uncertainties. The uncertainty band reflects the standard deviation of obtained cross-section values for 100 trials. All signals are labeled by the masses of the BSM particles except the $A \to BC$ signals, where $m_A = 3$ TeV, $m_B = 200$ GeV, and $m_C = 400$ GeV. Compared to the D_2^{trk}-defined regions, the anomaly SR performs competitively for all signals considered, and considerably better for the dark jet signal, indicating a high degree of signal-model-agnostic sensitivity. The red upward-pointing arrow for $A \to BC \to qqqqqq$ indicates that the limit obtained from the two-pronged (merged) SR lies above the upper edge of the plot.

for the $Y \to XH$ signals. Figure 13 provides a summary of the limits obtained from the signal injection tests, comparing all three signal region selections for the seven benchmark signal points. For points where the X particle is highly boosted and thus the anomaly score is most sensitive, the upper limit on the cross section is approximately the same across the merged and anomaly SRs. The D_2^{trk} selection for this analysis is a general one; further optimization of the D_2^{trk} selection would be expected to provide better performance than the anomaly score across two-prong simulated signals. However, the signal-model-independent aspect of the anomaly detection used in the anomaly SR is more evident through improved limits on the alternative substructure signals. Notably, for the dark jets the cross-section upper limit is nearly an order of magnitude lower than that provided by the two-prong regions, which underlines the particular strength of the model-independent approach for signals that are challenging to characterize with existing high-level variables.

While these results cover regions of phase space that have not been studied directly by other searches, some analysis selections overlap with those of other recent ATLAS dijet resonance searches. The m_X bin of [75.5, 95.5] GeV would be sensitive to a VH resonance's hadronic final state, which is covered by a dedicated analysis using the same dataset [72]. The present approach differs in the tagging techniques used for both the vector boson and Higgs boson but provides a similar 95% CL upper limit on the production cross section of a 3 TeV resonance. Due to its generality, the anomaly SR is expected to be sensitive to the same signatures as the weakly supervised dijet resonance search [13], but a direct comparison is not provided due to the assumptions made here about the mass and decay of the Higgs boson candidates.

XI. CONCLUSION

A search is performed for a heavy new boson Y decaying into a new particle X and a Standard Model Higgs boson in 139 fb^{-1} of 13 TeV pp collision data collected by the ATLAS detector during LHC run 2. The analysis focuses on a fully hadronic final state, where the X particle and H boson are boosted such that their daughter particles are collimated. In the first application of fully unsupervised machine learning to an ATLAS search, a VRNN is trained on jets in data to define an anomaly detection SR, which selects the X particle based solely on its substructural incompatibility with background jets. Two supplementary SRs are designed to separately reconstruct merged and resolved decays of a nominal two-prong X benchmark signal. Sensitivity over the dominant multijet background is enhanced by additional machine-learning applications, namely a NN-based $H \to b\bar{b}$ tagger and a DNN-based reweighting to ensure good modeling. No significant deviations of the data from the predicted background are observed. The largest excess is found in the anomaly SR with a global significance of 1.43σ when considering all m_X and m_Y bins and is not found to be compatible with the expected signal shape. Results are interpreted as 95% confidence-level upper limits on the cross section $\sigma(pp \to Y \to XH \to q\bar{q}b\bar{b})$, across the two-dimensional space where m_Y is between 1.5 and 6 TeV and m_X is between 65 and 3000 GeV. The most stringent upper limit of 0.341 fb is obtained in the merged SR for the signal point ($m_Y = 5000$ GeV, $m_X = 600$ GeV), while the weakest upper limit of 1.22 pb is obtained for the highly resolved point ($m_Y = 2500$ GeV, $m_X = 2000$ GeV).

ACKNOWLEDGMENTS

[1] ATLAS Collaboration, Observation of a new particle in the search for the Standard Model Higgs boson with the ATLAS detector at the LHC, Phys. Lett. B **716,** 1 (2012).

[2] CMS Collaboration, Observation of a new boson at a mass of 125 GeV with the CMS experiment at the LHC, Phys. Lett. B **716,** 30 (2012).

[3] G. Kasieczka *et al.*, The LHC Olympics 2020 a community challenge for anomaly detection in high energy physics, Rep. Prog. Phys. **84,** 124201 (2021).

[4] T. Aarrestad *et al.*, The dark machines anomaly score challenge: Benchmark data and model independent event classification for the large hadron collider, SciPost Phys. **12,** 043 (2022).

[5] G. Karagiorgi, G. Kasieczka, S. Kravitz, B. Nachman, and D. Shih, Machine learning in the search for new fundamental physics, arXiv:2112.03769.

[6] G. Altarelli, B. Mele, and M. Ruiz-Altaba, Searching for new heavy vector bosons in $p\bar{p}$ colliders, Z. Phys. C **45,** 109 (1989); **47,** 676(E) (1990).

[7] K. S. Agashe, Jack H. Collins, Peizhi Du, Sungwoo Hong, Doojin Kim, and Rashmish K. Mishra, LHC signals from cascade decays of warped vector resonances, J. High Energy Phys. 05 (2017) 078.

[8] L. Randall and R. Sundrum, Large Mass Hierarchy from a Small Extra Dimension, Phys. Rev. Lett. **83,** 3370 (1999).

[9] T. Han, J. D. Lykken, and R. J. Zhang, Kaluza-Klein states from large extra dimensions, Phys. Rev. D **59,** 105006 (1999).

[10] G. Branco, P. M. Ferreira, L. Lavoura, M. N. Rebelo, Marc Sher, and João P. Silva, Theory and phenomenology of two-Higgs-doublet models, Phys. Rep. **516,** 1 (2012).

[11] D. Pappadopulo, A. Thamm, R. Torre, and A. Wulzer, Heavy vector triplets: Bridging theory and data, J. High Energy Phys. 09 (2014) 060.

[12] ATLAS Collaboration, A search for resonances decaying into a Higgs boson and a new particle X in the XH → $qqbb$ final state with the ATLAS detector, Phys. Lett. B **779,** 24 (2018).

[13] ATLAS Collaboration, Dijet Resonance Search with Weak Supervision Using $\sqrt{s} = 13$ TeV pp collisions in the ATLAS detector, Phys. Rev. Lett. **125,** 131801 (2020).

[14] CMS Collaboration, Search for new heavy resonances decaying to WW, WZ, ZZ, WH, or ZH boson pairs in the all-jets final state in proton-proton collisions at $\sqrt{s} = 13$ TeV, Phys. Lett. B **844,** 137813 (2023).

[15] ATLAS Collaboration, The ATLAS Experiment at the CERN Large Hadron Collider, J. Instrum. **3**, S08003 (2008).

[16] ATLAS Collaboration, ATLAS insertable B-layer Technical Design Report No. ATLAS-TDR-19; , Report No. CERN-LHCC-2010-013, 2010; , Report No. CERN-LHCC-2012-009, 2012.

[17] B. Abbott *et al.*, Production and integration of the ATLAS insertable B-layer, J. Instrum. **13**, T05008 (2018).

[18] ATLAS Collaboration, The ATLAS Collaboration Software and Firmware, Report No. ATL-SOFT-PUB-2021-001, 2021.

[19] ATLAS Collaboration, ATLAS data quality operations and performance for 2015–2018 data-taking, J. Instrum. **15**, P04003 (2020).

[20] ATLAS Collaboration, Luminosity determination in pp collisions at $\sqrt{s} = 8$ TeV using the ATLAS detector at the LHC, Eur. Phys. J. C **76**, 653 (2016).

[21] G. Avoni *et al.*, The new LUCID-2 detector for luminosity measurement and monitoring in ATLAS, J. Instrum. **13**, P07017 (2018).

[22] ATLAS Collaboration, Topological cell clustering in the ATLAS calorimeters and its performance in LHC run 1, Eur. Phys. J. C **77**, 490 (2017).

[23] ATLAS Collaboration, The ATLAS simulation infrastructure, Eur. Phys. J. C **70**, 823 (2010).

[24] S. Agostinelli *et al.* (GEANT4 Collaboration), Geant4—a simulation toolkit, Nucl. Instrum. Methods Phys. Res., Sect. A **506**, 250 (2003).

[25] J. de Blas, J. M. Lizana, and M. Pérez-Victoria, Combining searches of Z' and W' bosons, J. High Energy Phys. 01 (2013) 166.

[26] J. Alwall, R. Frederix, S. Frixione, V. Hirschi, F. Maltoni, O. Mattelaer, H.-S. Shao, T. Stelzer, P. Torrielli, and M. Zaro, The automated computation of tree-level and next-to-leading order differential cross sections, and their matching to parton shower simulations, J. High Energy Phys. 07 (2014) 079.

[27] T. Sjöstrand, S. Mrenna, and P. Skands, A brief introduction to PYTHIA 8.1, Comput. Phys. Commun. **178**, 852 (2008).

[28] R. D. Ball *et al.*, Impact of heavy quark masses on parton distributions and LHC phenomenology, Nucl. Phys. **B849**, 296 (2011).

[29] ATLAS Collaboration, ATLAS Pythia 8 tunes to 7 TeV data, Technical Report No. ATL-PHYS-PUB-2014-021, CERN, 2014.

[30] ATLAS Collaboration, Search for diboson resonances in hadronic final states in 139 fb^{-1} of pp collisions at $\sqrt{s} = 13$ TeV with the ATLAS detector, J. High Energy Phys. 09 (2019) 091; 06 (2020) 42.

[31] M. Park and M. Zhang, Tagging a jet from a dark sector with jet substructure at colliders, Phys. Rev. D **100**, 115009 (2019).

[32] M. Cacciari, G. P. Salam, and G. Soyez, The anti-k_t jet clustering algorithm, J. High Energy Phys. 04 (2008) 063.

[33] M. Cacciari, G. P. Salam, and G. Soyez, FastJet user manual, Eur. Phys. J. C **72**, 1896 (2012).

[34] ATLAS Collaboration, Improving jet substructure performance in ATLAS using Track-CaloClusters, Technical Report No. ATL-PHYS-PUB-2017-015, CERN, 2017.

[35] D. Krohn, J. Thaler, and L.-T. Wang, Jet trimming, J. High Energy Phys. 02 (2010) 084.

[36] ATLAS Collaboration, Identification of boosted, hadronically-decaying W and Z bosons in $\sqrt{s} = 13$ TeV Monte Carlo simulations for ATLAS, Technical Report No. ATL-PHYS-PUB-2015-033, CERN, 2015.

[37] ATLAS Collaboration, Jet reconstruction and performance using particle flow with the ATLAS Detector, Eur. Phys. J. C **77**, 466 (2017).

[38] ATLAS Collaboration, Selection of jets produced in 13 TeV proton-proton collisions with the ATLAS detector, Technical Report No. ATLAS-CONF-2015-029, CERN, 2015.

[39] A. Kahn, J. Gonski, I. Ochoa, D. Williams, and G. Brooijmans, Anomalous jet identification via sequence modeling, J. Instrum. **16**, P08012 (2021).

[40] J. Chung *et al.*, A recurrent latent variable model for sequential data (2015), https://arxiv.org/abs/1506.02216.

[41] T. Heimel, G. Kasieczka, T. Plehn, and J. Thompson, QCD or what?, SciPost Phys. **6**, 030 (2019).

[42] M. Farina, Y. Nakai, and D. Shih, Searching for new physics with deep autoencoders, Phys. Rev. D **101**, 075021 (2020).

[43] B. Bortolato, A. Smolkovic, B. M. Dillon, and J. F. Kamenik, Bump hunting in latent space, Phys. Rev. D **105**, 115009 (2022).

[44] T. Cheng, J. F. Arguin, J. Leissner-Martin, J. Pilette, and T. Golling, Variational autoencoders for anomalous jet tagging, Phys. Rev. D **107**, 016002 (2023).

[45] A. Blance, M. Spannowsky, and P. Waite, Adversarially-trained autoencoders for robust unsupervised new physics searches, J. High Energy Phys. 10 (2019) 047.

[46] O. Cerri, T. Q. Nguyen, M. Pierini, M. Spiropulu, and J.-R. Vlimant, Variational autoencoders for new physics mining at the Large Hadron Collider, J. High Energy Phys. 05 (2019) 036.

[47] A. Paszke *et al.*, PyTorch: An imperative style, high-performance deep learning library, arXiv:1912.01703.

[48] D. P. Kingma and J. Ba, Adam: A method for stochastic optimization, arXiv:1412.6980.

[49] A. J. Larkoski, I. Moult, and D. Neill, Power counting to better jet observables, J. High Energy Phys. 12 (2014) 009.

[50] A. J. Larkoski, I. Moult, and D. Neill, Analytic boosted boson discrimination, J. High Energy Phys. 05 (2016) 117.

[51] J. Thaler and K. Van Tilburg, Identifying boosted objects with N-subjettiness, J. High Energy Phys. 03 (2011) 015.

[52] S. Marzani, G. Soyez, and M. Spannowsky, *Looking Inside Jets An Introduction to Jet Substructure and Boosted-object Phenomenology*, Lecture Notes in Physics (Springer, Cham, 2019).

[53] S. Kullback, *Information Theory and Statistics* (Wiley, New York, 1959), ISBN:978-0486696843.

[54] D. P. Kingma and M. Welling, Auto-encoding variational bayes, arXiv:1312.6114.

[55] ATLAS Collaboration, Identification of boosted Higgs bosons decaying Into $b\bar{b}$ with neural networks and variable radius subjets in ATLAS, Technical Report No. ATL-PHYS-PUB-2020-019, CERN, 2020.

[56] ATLAS Collaboration, ATLAS b-jet identification performance and efficiency measurement with $t\bar{t}$ events in pp collisions at $\sqrt{s} = 13$ TeV, Eur. Phys. J. C **79**, 970 (2019).

[57] D. Krohn, J. Thaler, and L.-T. Wang, Jets with variable R, J. High Energy Phys. 06 (2009) 059.

[58] T. Hastie, R. Tibshirani, and J. Friedman, *The Elements of Statistical Learning*, Springer Series in Statistics (Springer, New York, 2001).

[59] M. Sugiyama, T. Suzuki, and T. Kanamori, *Density Ratio Estimation in Machine Learning* (Cambridge University Press, Cambridge, England, 2012).

[60] B. Nachman and J. Thaler, Learning from many collider events at once, Phys. Rev. D **103,** 116013 (2021).

[61] F. Chollet *et al.*, Keras (2015), https://keras.io.

[62] Martín Abadi *et al.*, TensorFlow: Large-scale machine learning on heterogeneous systems, Software available from tensorflow.org (2015), arXiv:1603.04467.

[63] B. Efron, Bootstrap methods: Another look at the Jackknife, Ann. Stat. **7,** 1 (1979).

[64] U. Michelucci and F. Venturini, Estimating neural network's performance with bootstrap: A tutorial, Mach. Learn. Knowl. Extr. **3,** 357 (2021).

[65] ATLAS Collaboration, Luminosity determination in pp collisions at $\sqrt{s} = 13$ TeV using the ATLAS detector at the LHC, Technical Report, CERN, 2019.

[66] ATLAS Collaboration, Efficiency corrections for a tagger for boosted $H \rightarrow b\bar{b}$ decays in pp collisions at $\sqrt{s} = 13$ TeV with the ATLAS detector, Technical Report, CERN, 2021.

[67] ATLAS Collaboration, Performance of jet substructure techniques for large-R jets in proton–proton collisions at $\sqrt{s} = 7$ TeV using the ATLAS detector, J. High Energy Phys. 09 (2013) 076.

[68] ATLAS Collaboration, Jet energy scale and resolution measured in proton–proton collisions at $\sqrt{s} = 13$ TeV with the ATLAS detector, Eur. Phys. J. C **81,** 689 (2020).

[69] J. Butterworth *et al.*, PDF4LHC recommendations for LHC run II, J. Phys. G **43,** 023001 (2016).

[70] G. Choudalakis, On hypothesis testing, trials factor, hypertests and the BumpHunter, arXiv:1101.0390.

[71] A. L. Read, Presentation of search results: The CL_S technique, J. Phys. G **28,** 2693 (2002).

[72] ATLAS Collaboration, Search for resonances decaying into a weak vector boson and a Higgs boson in the fully hadronic final state produced in proton–proton collisions at $\sqrt{s} = 13$ TeV with the ATLAS detector, Phys. Rev. D **102,** 112008 (2020).

[73] ATLAS Collaboration, ATLAS computing acknowledgements, Report No. ATL-SOFT-PUB-2021-003, 2021.

G. Aad[101] B. Abbott[119] D. C. Abbott[102] K. Abeling[55] S. H. Abidi[29] A. Aboulhorma[35e] H. Abramowicz[150] H. Abreu[149] Y. Abulaiti[116] A. C. Abusleme Hoffman[136a] B. S. Acharya[68a,68b,b] B. Achkar[55] C. Adam Bourdarios[4] L. Adamczyk[84a] L. Adamek[154] S. V. Addepalli[26] J. Adelman[114] A. Adiguzel[21c] S. Adorni[56] T. Adye[133] A. A. Affolder[135] Y. Afik[36] M. N. Agaras[13] J. Agarwala[72a,72b] A. Aggarwal[99] C. Agheorghiesei[27c] J. A. Aguilar-Saavedra[129f] A. Ahmad[36] F. Ahmadov[38,c] W. S. Ahmed[103] S. Ahuja[94] X. Ai[48] G. Aielli[75a,75b] I. Aizenberg[168] M. Akbiyik[99] T. P. A. Åkesson[97] A. V. Akimov[37] K. Al Khoury[41] G. L. Alberghi[23b] J. Albert[164] P. Albicocco[53] S. Alderweireldt[52] M. Aleksa[36] I. N. Aleksandrov[38] C. Alexa[27b] T. Alexopoulos[10] A. Alfonsi[113] F. Alfonsi[23b] M. Alhroob[119] B. Ali[131] S. Ali[147] M. Aliev[37] G. Alimonti[70a] W. Alkakhi[55] C. Allaire[66] B. M. M. Allbrooke[145] P. P. Allport[20] A. Aloisio[71a,71b] F. Alonso[89] C. Alpigiani[137] E. Alunno Camelia[75a,75b] M. Alvarez Estevez[98] M. G. Alviggi[71a,71b] M. Aly[100] Y. Amaral Coutinho[81b] A. Ambler[103] C. Amelung[36] M. Amerl[1] C. G. Ames[108] D. Amidei[105] S. P. Amor Dos Santos[129a] S. Amoroso[48] K. R. Amos[162] V. Ananiev[124] C. Anastopoulos[138] T. Andeen[11] J. K. Anders[36] S. Y. Andrean[47a,47b] A. Andreazza[70a,70b] S. Angelidakis[9] A. Angerami[41,d] A. V. Anisenkov[37] A. Annovi[73a] C. Antel[56] M. T. Anthony[138] E. Antipov[120] M. Antonelli[53] D. J. A. Antrim[17a] F. Anulli[74a] M. Aoki[82] T. Aoki[152] J. A. Aparisi Pozo[162] M. A. Aparo[145] L. Aperio Bella[48] C. Appelt[18] N. Aranzabal[36] V. Araujo Ferraz[81a] C. Arcangeletti[53] A. T. H. Arce[51] E. Arena[91] J-F. Arguin[107] S. Argyropoulos[54] J.-H. Arling[48] A. J. Armbruster[36] O. Arnaez[154] H. Arnold[113] Z. P. Arrubarrena Tame[108] G. Artoni[74a,74b] H. Asada[110] K. Asai[117] S. Asai[152] N. A. Asbah[61] J. Assahsah[35d] K. Assamagan[29] R. Astalos[28a] R. J. Atkin[33a] M. Atkinson[161] N. B. Atlay[18] H. Atmani[62b] P. A. Atmasiddha[105] K. Augsten[131] S. Auricchio[71a,71b] A. D. Auriol[20] V. A. Austrup[170] G. Avner[149] G. Avolio[36] K. Axiotis[56] M. K. Ayoub[14c] G. Azuelos[107,e] D. Babal[28a] H. Bachacou[134] K. Bachas[151,f] A. Bachiu[34] F. Backman[47a,47b] A. Badea[61] P. Bagnaia[74a,74b] M. Bahmani[18] A. J. Bailey[162] V. R. Bailey[161] J. T. Baines[133] C. Bakalis[10] O. K. Baker[171] P. J. Bakker[113] E. Bakos[15] D. Bakshi Gupta[8] S. Balaji[146] R. Balasubramanian[113] E. M. Baldin[37] P. Balek[132] E. Ballabene[70a,70b] F. Balli[134] L. M. Baltes[63a] W. K. Balunas[32] J. Balz[99] E. Banas[85] M. Bandieramonte[128] A. Bandyopadhyay[24] S. Bansal[24] L. Barak[150] E. L. Barberio[104] D. Barberis[57b,57a] M. Barbero[101] G. Barbour[95] K. N. Barends[33a] T. Barillari[109] M-S. Barisits[36] T. Barklow[142] R. M. Barnett[17a] P. Baron[121] D. A. Baron Moreno[100] A. Baroncelli[62a] G. Barone[29] A. J. Barr[125] L. Barranco Navarro[47a,47b] F. Barreiro[98] J. Barreiro Guimarães da Costa[14a] U. Barron[150] M. G. Barros Teixeira[129a] S. Barsov[37] F. Bartels[63a]

R. Bartoldus[142] A. E. Barton[90] P. Bartos[28a] A. Basalaev[48] A. Basan[99] M. Baselga[49] I. Bashta[76a,76b]
A. Bassalat[66,g] M. J. Basso[154] C. R. Basson[100] R. L. Bates[59] S. Batlamous,[35e] J. R. Batley[32] B. Batool[140]
M. Battaglia[135] D. Battulga[18] M. Bauce[74a,74b] P. Bauer[24] A. Bayirli[21a] J. B. Beacham[51] T. Beau[126]
P. H. Beauchemin[157] F. Becherer[54] P. Bechtle[24] H. P. Beck[19,h] K. Becker[166] A. J. Beddall[21d]
V. A. Bednyakov[38] C. P. Bee[144] L. J. Beemster[15] T. A. Beermann[36] M. Begalli[81d] M. Begel[29] A. Behera[144]
J. K. Behr[48] C. Beirao Da Cruz E Silva[36] J. F. Beirer[55,36] F. Beisiegel[24] M. Belfkir[158] G. Bella[150]
L. Bellagamba[23b] A. Bellerive[34] P. Bellos[20] K. Beloborodov[37] K. Belotskiy[37] N. L. Belyaev[37]
D. Benchekroun[35a] F. Bendebba[35a] Y. Benhammou[150] D. P. Benjamin[29] M. Benoit[29] J. R. Bensinger[26]
S. Bentvelsen[113] L. Beresford[36] M. Beretta[53] D. Berge[18] E. Bergeaas Kuutmann[160] N. Berger[4]
B. Bergmann[131] J. Beringer[17a] S. Berlendis[7] G. Bernardi[5] C. Bernius[142] F. U. Bernlochner[24] T. Berry[94]
P. Berta[132] A. Berthold[50] I. A. Bertram[90] S. Bethke[109] A. Betti[74a,74b] A. J. Bevan[93] M. Bhamjee[33c]
S. Bhatta[144] D. S. Bhattacharya[165] P. Bhattarai[26] V. S. Bhopatkar[120] R. Bi,[29,i] R. M. Bianchi[128] O. Biebel[108]
R. Bielski[122] M. Biglietti[76a] T. R. V. Billoud[131] M. Bindi[55] A. Bingul[21b] C. Bini[74a,74b] S. Biondi[23b,23a]
A. Biondini[91] C. J. Birch-sykes[100] G. A. Bird[20,133] M. Birman[168] T. Bisanz[36] E. Bisceglie[43b,43a]
D. Biswas,[169,j] A. Bitadze[100] K. Bjørke[124] I. Bloch[48] C. Blocker[26] A. Blue[59] U. Blumenschein[93]
J. Blumenthal[99] G. J. Bobbink[113] V. S. Bobrovnikov[37] M. Boehler[54] D. Bogavac[36] A. G. Bogdanchikov[37]
C. Bohm[47a] V. Boisvert[94] P. Bokan[48] T. Bold[84a] M. Bomben[5] M. Bona[93] M. Boonekamp[134]
C. D. Booth[94] A. G. Borbély[59] H. M. Borecka-Bielska[107] L. S. Borgna[95] G. Borissov[90] D. Bortoletto[125]
D. Boscherini[23b] M. Bosman[13] J. D. Bossio Sola[36] K. Bouaouda[35a] N. Bouchhar[162] J. Boudreau[128]
E. V. Bouhova-Thacker[90] D. Boumediene[40] R. Bouquet[5] A. Boveia[118] J. Boyd[36] D. Boye[29] I. R. Boyko[38]
J. Bracinik[20] N. Brahimi[62d] G. Brandt[170] O. Brandt[32] F. Braren[48] B. Brau[102] J. E. Brau[122]
K. Brendlinger[48] R. Brener[168] L. Brenner[113] R. Brenner[160] S. Bressler[168] B. Brickwedde[99] D. Britton[59]
D. Britzger[109] I. Brock[24] G. Brooijmans[41] W. K. Brooks[136f] E. Brost[29] T. L. Bruckler[125]
P. A. Bruckman de Renstrom[85] B. Brüers[48] D. Bruncko,[28b,a] A. Bruni[23b] G. Bruni[23b] M. Bruschi[23b]
N. Bruscino[74a,74b] L. Bryngemark[142] T. Buanes[16] Q. Buat[137] P. Buchholz[140] A. G. Buckley[59]
I. A. Budagov,[38,a] M. K. Bugge[124] O. Bulekov[37] B. A. Bullard[61] S. Burdin[91] C. D. Burgard[48]
A. M. Burger[40] B. Burghgrave[8] J. T. P. Burr[32] C. D. Burton[11] J. C. Burzynski[141] E. L. Busch[41] V. Büscher[99]
P. J. Bussey[59] J. M. Butler[25] C. M. Buttar[59] J. M. Butterworth[95] W. Buttinger[133] C. J. Buxo Vazquez,[106]
A. R. Buzykaev[37] G. Cabras[23b] S. Cabrera Urbán[162] D. Caforio[58] H. Cai[128] Y. Cai[14a,14d] V. M. M. Cairo[36]
O. Cakir[3a] N. Calace[36] P. Calafiura[17a] G. Calderini[126] P. Calfayan[67] G. Callea[59] L. P. Caloba,[81b] D. Calvet[40]
S. Calvet[40] T. P. Calvet[101] M. Calvetti[73a,73b] R. Camacho Toro[126] S. Camarda[36] D. Camarero Munoz[26]
P. Camarri[75a,75b] M. T. Camerlingo[76a,76b] D. Cameron[124] C. Camincher[164] M. Campanelli[95] A. Camplani[42]
V. Canale[71a,71b] A. Canesse[103] M. Cano Bret[79] J. Cantero[162] Y. Cao[161] F. Capocasa[26] M. Capua[43b,43a]
A. Carbone[70a,70b] R. Cardarelli[75a] J. C. J. Cardenas[8] F. Cardillo[162] T. Carli[36] G. Carlino[71a] J. I. Carlotto[13]
B. T. Carlson,[128,k] E. M. Carlson[164,155a] L. Carminati[70a,70b] M. Carnesale[74a,74b] S. Caron[112] E. Carquin[136f]
S. Carrá[70a,70b] G. Carratta[23b,23a] F. Carrio Argos[33g] J. W. S. Carter[154] T. M. Carter[52] M. P. Casado,[13,l]
A. F. Casha,[154] E. G. Castiglia[171] F. L. Castillo[63a] L. Castillo Garcia[13] V. Castillo Gimenez[162] N. F. Castro[129a,129e]
A. Catinaccio[36] J. R. Catmore[124] V. Cavaliere[29] N. Cavalli[23b,23a] V. Cavasinni[73a,73b] E. Celebi[21a] F. Celli[125]
M. S. Centonze[69a,69b] K. Cerny[121] A. S. Cerqueira[81a] A. Cerri[145] L. Cerrito[75a,75b] F. Cerutti[17a] A. Cervelli[23b]
S. A. Cetin[21d] Z. Chadi[35a] D. Chakraborty[114] M. Chala[129f] J. Chan[169] W. Y. Chan[152] J. D. Chapman[32]
B. Chargeishvili[148b] D. G. Charlton[20] T. P. Charman[93] M. Chatterjee[19] S. Chekanov[6] S. V. Chekulaev[155a]
G. A. Chelkov,[38,m] A. Chen[105] B. Chen[150] B. Chen[164] H. Chen[14c] H. Chen[29] J. Chen[62c] J. Chen[26]
S. Chen[152] S. J. Chen[14c] X. Chen[62c] X. Chen,[14b,n] Y. Chen[62a] C. L. Cheng[169] H. C. Cheng[64a] S. Cheong[142]
A. Cheplakov[38] E. Cheremushkina[48] E. Cherepanova[113] R. Cherkaoui El Moursli[35e] E. Cheu[7] K. Cheung[65]
L. Chevalier[134] V. Chiarella[53] G. Chiarelli[73a] N. Chiedde[101] G. Chiodini[69a] A. S. Chisholm[20] A. Chitan[27b]
M. Chitishvili[162] Y. H. Chiu[164] M. V. Chizhov[38] K. Choi[11] A. R. Chomont[74a,74b] Y. Chou[102]
E. Y. S. Chow[113] T. Chowdhury[33g] L. D. Christopher[33g] K. L. Chu[64a] M. C. Chu[64a] X. Chu[14a,14d]
J. Chudoba[130] J. J. Chwastowski[85] D. Cieri[109] K. M. Ciesla[84a] V. Cindro[92] A. Ciocio[17a] F. Cirotto[71a,71b]
Z. H. Citron,[168,o] M. Citterio[70a] D. A. Ciubotaru[27b] B. M. Ciungu[154] A. Clark[56] P. J. Clark[52]

J. M. Clavijo Columbie[48] S. E. Clawson[100] C. Clement[47a,47b] J. Clercx[48] L. Clissa[23b,23a] Y. Coadou[101] M. Cobal[68a,68c] A. Coccaro[57b] R. F. Coelho Barrue[129a] R. Coelho Lopes De Sa[102] S. Coelli[70a] H. Cohen[150] A. E. C. Coimbra[70a,70b] B. Cole[41] J. Collot[60] P. Conde Muiño[129a,129g] M. P. Connell[33c] S. H. Connell[33c] I. A. Connelly[59] E. I. Conroy[125] F. Conventi[71a,p] H. G. Cooke[20] A. M. Cooper-Sarkar[125] F. Cormier[163] L. D. Corpe[36] M. Corradi[74a,74b] E. E. Corrigan[97] F. Corriveau[103,q] A. Cortes-Gonzalez[18] M. J. Costa[162] F. Costanza[4] D. Costanzo[138] B. M. Cote[118] G. Cowan[94] J. W. Cowley[32] K. Cranmer[116] S. Crépé-Renaudin[60] F. Crescioli[126] M. Cristinziani[140] M. Cristoforetti[77a,77b,r] V. Croft[157] G. Crosetti[43b,43a] A. Cueto[36] T. Cuhadar Donszelmann[159] H. Cui[14a,14d] Z. Cui[7] A. R. Cukierman[142] W. R. Cunningham[59] F. Curcio[43b,43a] P. Czodrowski[36] M. M. Czurylo[63b] M. J. Da Cunha Sargedas De Sousa[62a] J. V. Da Fonseca Pinto[81b] C. Da Via[100] W. Dabrowski[84a] T. Dado[49] S. Dahbi[33g] T. Dai[105] C. Dallapiccola[102] M. Dam[42] G. D'amen[29] V. D'Amico[108] J. Damp[99] J. R. Dandoy[127] M. F. Daneri[30] M. Danninger[141] V. Dao[36] G. Darbo[57b] S. Darmora[6] S. J. Das[29,i] S. D'Auria[70a,70b] A. D'avanzo[71b] C. David[155b] T. Davidek[132] D. R. Davis[51] B. Davis-Purcell[34] I. Dawson[93] K. De[8] R. De Asmundis[71a] M. De Beurs[113] N. De Biase[48] S. De Castro[23b,23a] N. De Groot[112] P. de Jong[113] H. De la Torre[106] A. De Maria[14c] A. De Salvo[74a] U. De Sanctis[75a,75b] A. De Santo[145] J. B. De Vivie De Regie[60] D. V. Dedovich,[38] J. Degens[113] A. M. Deiana[44] F. Del Corso[23b,23a] J. Del Peso[98] F. Del Rio[63a] F. Deliot[134] C. M. Delitzsch[49] M. Della Pietra[71a,71b] D. Della Volpe[56] A. Dell'Acqua[36] L. Dell'Asta[70a,70b] M. Delmastro[4] P. A. Delsart[60] S. Demers[171] M. Demichev[38] S. P. Denisov[37] L. D'Eramo[114] D. Derendarz[85] F. Derue[126] P. Dervan[91] K. Desch[24] K. Dette[154] C. Deutsch[24] P. O. Deviveiros[36] F. A. Di Bello[57b,57a] A. Di Ciaccio[75a,75b] L. Di Ciaccio[4] A. Di Domenico[74a,74b] C. Di Donato[71a,71b] A. Di Girolamo[36] G. Di Gregorio[5] A. Di Luca[77a,77b] B. Di Micco[76a,76b] R. Di Nardo[76a,76b] C. Diaconu[101] F. A. Dias[113] T. Dias Do Vale[141] M. A. Diaz[136a,136b] F. G. Diaz Capriles[24] M. Didenko[162] E. B. Diehl[105] L. Diehl[54] S. Díez Cornell[48] C. Diez Pardos[140] C. Dimitriadi[24,160] A. Dimitrievska[17a] W. Ding[14b] J. Dingfelder[24] I-M. Dinu[27b] S. J. Dittmeier[63b] F. Dittus[36] F. Djama[101] T. Djobava[148b] J. I. Djuvsland[16] C. Doglioni[100,97] J. Dolejsi[132] Z. Dolezal[132] M. Donadelli[81c] B. Dong[62c] J. Donini[40] A. D'Onofrio[14c] M. D'Onofrio[91] J. Dopke[133] A. Doria[71a] M. T. Dova[89] A. T. Doyle[59] M. A. Draguet[125] E. Drechsler[141] E. Dreyer[168] I. Drivas-koulouris[10] A. S. Drobac[157] M. Drozdova[56] D. Du[62a] T. A. du Pree[113] F. Dubinin[37] M. Dubovsky[28a] E. Duchovni[168] G. Duckeck[108] O. A. Ducu[27b] D. Duda[109] A. Dudarev[36] M. D'uffizi[100] L. Duflot[66] M. Dührssen[36] C. Dülsen[170] A. E. Dumitriu[27b] M. Dunford[63a] S. Dungs[49] K. Dunne[47a,47b] A. Duperrin[101] H. Duran Yildiz[3a] M. Düren[58] A. Durglishvili[148b] B. L. Dwyer[114] G. I. Dyckes[17a] M. Dyndal[84a] S. Dysch[100] B. S. Dziedzic[85] Z. O. Earnshaw[145] B. Eckerova[28a] M. G. Eggleston,[51] E. Egidio Purcino De Souza[81b] L. F. Ehrke[56] G. Eigen[16] K. Einsweiler[17a] T. Ekelof[160] P. A. Ekman[97] Y. El Ghazali[35b] H. El Jarrari[35e,147] A. El Moussaouy[35a] V. Ellajosyula[160] M. Ellert[160] F. Ellinghaus[170] A. A. Elliot[93] N. Ellis[36] J. Elmsheuser[29] M. Elsing[36] D. Emeliyanov[133] A. Emerman[41] Y. Enari[152] I. Ene[17a] S. Epari[13] J. Erdmann[49,s] A. Ereditato[19] P. A. Erland[85] M. Errenst[170] M. Escalier[66] C. Escobar[162] E. Etzion[150] G. Evans[129a] H. Evans[67] M. O. Evans[145] A. Ezhilov[37] S. Ezzarqtouni[35a] F. Fabbri[59] L. Fabbri[23b,23a] G. Facini[95] V. Fadeyev[135] R. M. Fakhrutdinov[37] S. Falciano[74a] P. J. Falke[24] S. Falke[36] J. Faltova[132] Y. Fan[14a] Y. Fang[14a,14d] G. Fanourakis[46] M. Fanti[70a,70b] M. Faraj[68a,68b] Z. Farazpay,[96] A. Farbin[8] A. Farilla[76a] T. Farooque[106] S. M. Farrington[52] F. Fassi[35e] D. Fassouliotis[9] M. Faucci Giannelli[75a,75b] W. J. Fawcett[32] L. Fayard[66] P. Federicova[130] O. L. Fedin[37,m] G. Fedotov[37] M. Feickert[169] L. Feligioni[101] A. Fell[138] D. E. Fellers[122] C. Feng[62b] M. Feng[14b] Z. Feng[113] M. J. Fenton[159] A. B. Fenyuk,[37] L. Ferencz[48] S. W. Ferguson[45] J. Ferrando[48] A. Ferrari[160] P. Ferrari[113,112] R. Ferrari[72a] D. Ferrere[56] C. Ferretti[105] F. Fiedler[99] A. Filipčič[92] E. K. Filmer[1] F. Filthaut[112] M. C. N. Fiolhais[129a,129c,t] L. Fiorini[162] F. Fischer[140] W. C. Fisher[106] T. Fitschen[100] I. Fleck[140] P. Fleischmann[105] T. Flick[170] L. Flores[127] M. Flores[33d,u] L. R. Flores Castillo[64a] F. M. Follega[77a,77b] N. Fomin[16] J. H. Foo[154] B. C. Forland,[67] A. Formica[134] A. C. Forti[100] E. Fortin[101] A. W. Fortman[61] M. G. Foti[17a] L. Fountas[9,v] D. Fournier[66] H. Fox[90] P. Francavilla[73a,73b] S. Francescato[61] S. Franchellucci[56] M. Franchini[23b,23a] S. Franchino[63a] D. Francis,[36] L. Franco[112] L. Franconi[19] M. Franklin[61] G. Frattari[26] A. C. Freegard[93] P. M. Freeman[20] W. S. Freund[81b] N. Fritzsche[50] A. Froch[54] D. Froidevaux[36] J. A. Frost[125] Y. Fu[62a] M. Fujimoto[117] E. Fullana Torregrosa[162,a]

J. Fuster[162] A. Gabrielli[23b,23a] A. Gabrielli[154] P. Gadow[48] G. Gagliardi[57b,57a] L. G. Gagnon[17a]
G. E. Gallardo[125] E. J. Gallas[125] B. J. Gallop[133] R. Gamboa Goni[93] K. K. Gan[118] S. Ganguly[152] J. Gao[62a]
Y. Gao[52] F. M. Garay Walls[136a,136b] B. Garcia[29,i] C. García[162] J. E. García Navarro[162] J. A. García Pascual[14a]
M. Garcia-Sciveres[17a] R. W. Gardner[39] D. Garg[79] R. B. Garg[142,w] S. Gargiulo[54] C. A. Garner[154] V. Garonne[29]
S. J. Gasiorowski[137] P. Gaspar[81b] G. Gaudio[72a] V. Gautam[13] P. Gauzzi[74a,74b] I. L. Gavrilenko[37] A. Gavrilyuk[37]
C. Gay[163] G. Gaycken[48] E. N. Gazis[10] A. A. Geanta[27b,27e] C. M. Gee[135] J. Geisen[97] M. Geisen[99]
C. Gemme[57b] M. H. Genest[60] S. Gentile[74a,74b] S. George[94] W. F. George[20] T. Geralis[46] L. O. Gerlach[55]
P. Gessinger-Befurt[36] M. Ghasemi Bostanabad[164] M. Ghneimat[140] K. Ghorbanian[93] A. Ghosal[140] A. Ghosh[159]
A. Ghosh[7] B. Giacobbe[23b] S. Giagu[74a,74b] N. Giangiacomi[154] P. Giannetti[73a] A. Giannini[62a] S. M. Gibson[94]
M. Gignac[135] D. T. Gil[84b] A. K. Gilbert[84a] B. J. Gilbert[41] D. Gillberg[34] G. Gilles[113] N. E. K. Gillwald[48]
L. Ginabat[126] D. M. Gingrich[2,e] M. P. Giordani[68a,68c] P. F. Giraud[134] G. Giugliarelli[68a,68c] D. Giugni[70a]
F. Giuli[36] I. Gkialas[9,v] L. K. Gladilin[37] C. Glasman[98] G. R. Gledhill[122] M. Glisic,[122] I. Gnesi[43b,x] Y. Go[29,i]
M. Goblirsch-Kolb[26] B. Gocke[49] D. Godin[107] S. Goldfarb[104] T. Golling[56] M. G. D. Gololo[33g] D. Golubkov[37]
J. P. Gombas[106] A. Gomes[129a,129b] G. Gomes Da Silva[140] A. J. Gomez Delegido[162] R. Goncalves Gama[55]
R. Gonçalo[129a,129c] G. Gonella[122] L. Gonella[20] A. Gongadze[38] F. Gonnella[20] J. L. Gonski[41]
R. Y. González Andana[52] S. González de la Hoz[162] S. Gonzalez Fernandez[13] R. Gonzalez Lopez[91]
C. Gonzalez Renteria[17a] R. Gonzalez Suarez[160] S. Gonzalez-Sevilla[56] G. R. Gonzalvo Rodriguez[162]
L. Goossens[36] N. A. Gorasia[20] P. A. Gorbounov[37] B. Gorini[36] E. Gorini[69a,69b] A. Gorišek[92] A. T. Goshaw[51]
M. I. Gostkin[38] C. A. Gottardo[36] M. Gouighri[35b] V. Goumarre[48] A. G. Goussiou[137] N. Govender[33c] C. Goy[4]
I. Grabowska-Bold[84a] K. Graham[34] E. Gramstad[124] S. Grancagnolo[18] M. Grandi[145] V. Gratchev,[37,a]
P. M. Gravila[27f] F. G. Gravili[69a,69b] H. M. Gray[17a] M. Greco[69a,69b] C. Grefe[24] I. M. Gregor[48] P. Grenier[142]
C. Grieco[13] A. A. Grillo[135] K. Grimm[31,y] S. Grinstein[13,z] J.-F. Grivaz[66] E. Gross[168] J. Grosse-Knetter[55]
C. Grud,[105] A. Grummer[111] J. C. Grundy[125] L. Guan[105] W. Guan[169] C. Gubbels[163] J. G. R. Guerrero Rojas[162]
G. Guerrieri[68a,68b] F. Guescini[109] R. Gugel[99] J. A. M. Guhit[105] A. Guida[48] T. Guillemin[4] E. Guilloton[166,133]
S. Guindon[36] F. Guo[14a,14d] J. Guo[62c] L. Guo[66] Y. Guo[105] R. Gupta[48] S. Gurbuz[24] S. S. Gurdasani[54]
G. Gustavino[36] M. Guth[56] P. Gutierrez[119] L. F. Gutierrez Zagazeta[127] C. Gutschow[95] C. Guyot[134]
C. Gwenlan[125] C. B. Gwilliam[91] E. S. Haaland[124] A. Haas[116] M. Habedank[48] C. Haber[17a] H. K. Hadavand[8]
A. Hadef[99] S. Hadzic[109] E. H. Haines[95] M. Haleem[165] J. Haley[120] J. J. Hall[138] G. D. Hallewell[101]
L. Halser[19] K. Hamano[164] H. Hamdaoui[35e] M. Hamer[24] G. N. Hamity[52] J. Han[62b] K. Han[62a] L. Han[14c]
L. Han[62a] S. Han[17a] Y. F. Han[154] K. Hanagaki[82] M. Hance[135] D. A. Hangal[41,d] H. Hanif[141] M. D. Hank[39]
R. Hankache[100] J. B. Hansen[42] J. D. Hansen[42] P. H. Hansen[42] K. Hara[156] D. Harada[56] T. Harenberg[170]
S. Harkusha[37] Y. T. Harris[125] N. M. Harrison[118] P. F. Harrison,[166] N. M. Hartman[142] N. M. Hartmann[108]
Y. Hasegawa[139] A. Hasib[52] S. Haug[19] R. Hauser[106] M. Havranek[131] C. M. Hawkes[20] R. J. Hawkings[36]
S. Hayashida[110] D. Hayden[106] C. Hayes[105] R. L. Hayes[163] C. P. Hays[125] J. M. Hays[93] H. S. Hayward[91]
F. He[62a] Y. He[153] Y. He[126] M. P. Heath[52] V. Hedberg[97] A. L. Heggelund[124] N. D. Hehir[93] C. Heidegger[54]
K. K. Heidegger[54] W. D. Heidorn[80] J. Heilman[34] S. Heim[48] T. Heim[17a] J. G. Heinlein[127] J. J. Heinrich[122]
L. Heinrich,[109,aa] J. Hejbal[130] L. Helary[48] A. Held[169] S. Hellesund[124] C. M. Helling[163] S. Hellman[47a,47b]
C. Helsens[36] R. C. W. Henderson,[90] L. Henkelmann[32] A. M. Henriques Correia,[36] H. Herde[97]
Y. Hernández Jiménez[144] L. M. Herrmann[24] M. G. Herrmann[108] T. Herrmann[50] G. Herten[54]
R. Hertenberger[108] L. Hervas[36] N. P. Hessey[155a] H. Hibi[83] E. Higón-Rodriguez[162] S. J. Hillier[20]
I. Hinchliffe[17a] F. Hinterkeuser[24] M. Hirose[123] S. Hirose[156] D. Hirschbuehl[170] T. G. Hitchings[100] B. Hiti[92]
J. Hobbs[144] R. Hobincu[27e] N. Hod[168] M. C. Hodgkinson[138] B. H. Hodkinson[32] A. Hoecker[36] J. Hofer[48]
D. Hohn[54] T. Holm[24] M. Holzbock[109] L. B. A. H. Hommels[32] B. P. Honan[100] J. Hong[62c] T. M. Hong[128]
J. C. Honig[54] A. Hönle[109] B. H. Hooberman[161] W. H. Hopkins[6] Y. Horii[110] S. Hou[147] A. S. Howard[92]
J. Howarth[59] J. Hoya[6] M. Hrabovsky[121] A. Hrynevich[48] T. Hryn'ova[4] P. J. Hsu[65] S.-C. Hsu[137] Q. Hu[41]
Y. F. Hu[14a,14d,bb] D. P. Huang[95] S. Huang[64b] X. Huang[14c] Y. Huang[62a] Y. Huang[14a] Z. Huang[100]
Z. Hubacek[131] M. Huebner[24] F. Huegging[24] T. B. Huffman[125] M. Huhtinen[36] S. K. Huiberts[16]
R. Hulsken[103] N. Huseynov[12,m] J. Huston[106] J. Huth[61] R. Hyneman[142] S. Hyrych[28a] G. Iacobucci[56]
G. Iakovidis[29] I. Ibragimov[140] L. Iconomidou-Fayard[66] P. Iengo[71a,71b] R. Iguchi[152] T. Iizawa[56] Y. Ikegami[82]

A. Ilg[19] N. Ilic[154] H. Imam[35a] T. Ingebretsen Carlson[47a,47b] G. Introzzi[72a,72b] M. Iodice[76a] V. Ippolito[74a,74b] M. Ishino[152] W. Islam[169] C. Issever[18,48] S. Istin[21a,cc] H. Ito[167] J. M. Iturbe Ponce[64a] R. Iuppa[77a,77b] A. Ivina[168] J. M. Izen[45] V. Izzo[71a] P. Jacka[130,131] P. Jackson[1] R. M. Jacobs[48] B. P. Jaeger[141] C. S. Jagfeld[108] G. Jäkel[170] K. Jakobs[54] T. Jakoubek[168] J. Jamieson[59] K. W. Janas[84a] G. Jarlskog[97] A. E. Jaspan[91] M. Javurkova[102] F. Jeanneau[134] L. Jeanty[122] J. Jejelava[148a,dd] P. Jenni[54,ee] C. E. Jessiman[34] S. Jézéquel[4] J. Jia[144] X. Jia[61] X. Jia[14a,14d] Z. Jia[14c] Y. Jiang[62a] S. Jiggins[52] J. Jimenez Pena[109] S. Jin[14c] A. Jinaru[27b] O. Jinnouchi[153] P. Johansson[138] K. A. Johns[7] D. M. Jones[32] E. Jones[166] P. Jones[32] R. W. L. Jones[90] T. J. Jones[91] R. Joshi[118] J. Jovicevic[15] X. Ju[17a] J. J. Junggeburth[36] A. Juste Rozas[13,z] S. Kabana[136e] A. Kaczmarska[85] M. Kado[74a,74b] H. Kagan[118] M. Kagan[142] A. Kahn[41] A. Kahn[127] C. Kahra[99] T. Kaji[167] E. Kajomovitz[149] N. Kakati[168] C. W. Kalderon[29] A. Kamenshchikov[154] S. Kanayama[153] N. J. Kang[135] Y. Kano[110] D. Kar[33g] K. Karava[125] M. J. Kareem[155b] E. Karentzos[54] I. Karkanias[151,ff] S. N. Karpov[38] Z. M. Karpova[38] V. Kartvelishvili[90] A. N. Karyukhin[37] E. Kasimi[151,ff] C. Kato[62d] J. Katzy[48] S. Kaur[34] K. Kawade[139] K. Kawagoe[88] T. Kawamoto[134] G. Kawamura[55] E. F. Kay[164] F. I. Kaya[157] S. Kazakos[13] V. F. Kazanin[37] Y. Ke[144] J. M. Keaveney[33a] R. Keeler[164] G. V. Kehris[61] J. S. Keller[34] A. S. Kelly[95] D. Kelsey[145] J. J. Kempster[20] K. E. Kennedy[41] P. D. Kennedy[99] O. Kepka[130] B. P. Kerridge[166] S. Kersten[170] B. P. Kerševan[92] S. Keshri[66] L. Keszeghova[28a] S. Ketabchi Haghighat[154] M. Khandoga[126] A. Khanov[120] A. G. Kharlamov[37] T. Kharlamova[37] E. E. Khoda[137] T. J. Khoo[18] G. Khoriauli[165] J. Khubua[148b] Y. A. R. Khwaira[66] M. Kiehn[36] A. Kilgallon[122] D. W. Kim[47a,47b] E. Kim[153] Y. K. Kim[39] N. Kimura[95] A. Kirchhoff[55] D. Kirchmeier[50] C. Kirfel[24] J. Kirk[133] A. E. Kiryunin[109] T. Kishimoto[152] D. P. Kisliuk[154] C. Kitsaki[10] O. Kivernyk[24] M. Klassen[63a] C. Klein[34] L. Klein[165] M. H. Klein[105] M. Klein[91] S. B. Klein[56] U. Klein[91] P. Klimek[36] A. Klimentov[29] F. Klimpel[109] T. Klingl[24] T. Klioutchnikova[36] F. F. Klitzner[108] P. Kluit[113] S. Kluth[109] E. Kneringer[78] T. M. Knight[154] A. Knue[54] D. Kobayashi[88] R. Kobayashi[86] M. Kocian[142] P. Kodyš[132] D. M. Koeck[145] P. T. Koenig[24] T. Koffas[34] M. Kolb[134] I. Koletsou[4] T. Komarek[121] K. Köneke[54] A. X. Y. Kong[1] T. Kono[117] N. Konstantinidis[95] B. Konya[97] R. Kopeliansky[67] S. Koperny[84a] K. Korcyl[85] K. Kordas[151,ff] G. Koren[150] A. Korn[95] S. Korn[55] I. Korolkov[13] N. Korotkova[37] B. Kortman[113] O. Kortner[109] S. Kortner[109] W. H. Kostecka[114] V. V. Kostyukhin[140] A. Kotsokechagia[134] A. Kotwal[51] A. Koulouris[36] A. Kourkoumeli-Charalampidi[72a,72b] C. Kourkoumelis[9] E. Kourlitis[6] O. Kovanda[145] R. Kowalewski[164] W. Kozanecki[134] A. S. Kozhin[37] V. A. Kramarenko[37] G. Kramberger[92] P. Kramer[99] M. W. Krasny[126] A. Krasznahorkay[36] J. A. Kremer[99] T. Kresse[50] J. Kretzschmar[91] K. Kreul[18] P. Krieger[154] F. Krieter[108] S. Krishnamurthy[102] A. Krishnan[63b] M. Krivos[132] K. Krizka[17a] K. Kroeninger[49] H. Kroha[109] J. Kroll[130] J. Kroll[127] K. S. Krowpman[106] U. Kruchonak[38] H. Krüger[24] N. Krumnack[80] M. C. Kruse[51] J. A. Krzysiak[85] O. Kuchinskaia[37] S. Kuday[3a] D. Kuechler[48] J. T. Kuechler[48] S. Kuehn[36] T. Kuhl[48] V. Kukhtin[38] Y. Kulchitsky[37,m] S. Kuleshov[136d,136b] M. Kumar[33g] N. Kumari[101] A. Kupco[130] T. Kupfer[49] A. Kupich[37] O. Kuprash[54] H. Kurashige[83] L. L. Kurchaninov[155a] Y. A. Kurochkin[37] A. Kurova[37] M. Kuze[153] A. K. Kvam[102] J. Kvita[121] T. Kwan[103] K. W. Kwok[64a] N. G. Kyriacou[105] L. A. O. Laatu[101] C. Lacasta[162] F. Lacava[74a,74b] H. Lacker[18] D. Lacour[126] N. N. Lad[95] E. Ladygin[38] B. Laforge[126] T. Lagouri[136e] S. Lai[55] I. K. Lakomiec[84a] N. Lalloue[60] J. E. Lambert[119] S. Lammers[67] W. Lampl[7] C. Lampoudis[151,ff] A. N. Lancaster[114] E. Lançon[29] U. Landgraf[54] M. P. J. Landon[93] V. S. Lang[54] R. J. Langenberg[102] A. J. Lankford[159] F. Lanni[36] K. Lantzsch[24] A. Lanza[72a] A. Lapertosa[57b,57a] J. F. Laporte[134] T. Lari[70a] F. Lasagni Manghi[23b] M. Lassnig[36] V. Latonova[130] T. S. Lau[64a] A. Laudrain[99] A. Laurier[34] S. D. Lawlor[94] Z. Lawrence[100] M. Lazzaroni[70a,70b] B. Le[100] B. Leban[92] A. Lebedev[80] M. LeBlanc[36] T. LeCompte[6] F. Ledroit-Guillon[60] A. C. A. Lee[95] G. R. Lee[16] L. Lee[61] S. C. Lee[147] S. Lee[47a,47b] T. F. Lee[91] L. L. Leeuw[33c] H. P. Lefebvre[94] M. Lefebvre[164] C. Leggett[17a] K. Lehmann[141] G. Lehmann Miotto[36] M. Leigh[56] W. A. Leight[102] A. Leisos[151,gg] M. A. L. Leite[81c] C. E. Leitgeb[48] R. Leitner[132] K. J. C. Leney[44] T. Lenz[24] S. Leone[73a] C. Leonidopoulos[52] A. Leopold[143] C. Leroy[107] R. Les[106] C. G. Lester[32] M. Levchenko[37] J. Levêque[4] D. Levin[105] L. J. Levinson[168] M. P. Lewicki[85] D. J. Lewis[4] A. Li[5] B. Li[14b] B. Li[62b] C. Li[62a] C-Q. Li[62c] H. Li[62a] H. Li[62b] H. Li[14c] H. Li[62b] J. Li[62c] K. Li[137] L. Li[62c] M. Li[14a,14d] Q. Y. Li[62a] S. Li[14a,14d] S. Li[62d,62c,hh] T. Li[62b] X. Li[103] Z. Li[62b] Z. Li[125] Z. Li[103] Z. Li[91] Z. Li[14a,14d] Z. Liang[14a] M. Liberatore[48] B. Liberti[75a] K. Lie[64c]

J. Lieber Marin [81b] K. Lin [106] R. A. Linck [67] R. E. Lindley [7] J. H. Lindon [2] A. Linss [48] E. Lipeles [127] A. Lipniacka [16] A. Lister [163] J. D. Little [4] B. Liu [14a] B. X. Liu [141] D. Liu [62d,62c] J. B. Liu [62a] J. K. K. Liu [32] K. Liu [62d,62c] M. Liu [62a] M. Y. Liu [62a] P. Liu [14a] Q. Liu [62d,137,62c] X. Liu [62a] Y. Liu [48] Y. Liu [14c,14d] Y. L. Liu [105] Y. W. Liu [62a] M. Livan [72a,72b] J. Llorente Merino [141] S. L. Lloyd [93] E. M. Lobodzinska [48] P. Loch [7] S. Loffredo [75a,75b] T. Lohse [18] K. Lohwasser [138] M. Lokajicek [130,a] J. D. Long [161] I. Longarini [74a,74b] L. Longo [69a,69b] R. Longo [161] I. Lopez Paz [36] A. Lopez Solis [48] J. Lorenz [108] N. Lorenzo Martinez [4] A. M. Lory [108] A. Lösle [54] X. Lou [47a,47b] X. Lou [14a,14d] A. Lounis [66] J. Love [6] P. A. Love [90] J. J. Lozano Bahilo [162] G. Lu [14a,14d] M. Lu [79] S. Lu [127] Y. J. Lu [65] H. J. Lubatti [137] C. Luci [74a,74b] F. L. Lucio Alves [14c] A. Lucotte [60] F. Luehring [67] I. Luise [144] O. Lukianchuk [66] O. Lundberg [143] B. Lund-Jensen [143] N. A. Luongo [122] M. S. Lutz [150] D. Lynn [29] H. Lyons [91] R. Lysak [130] E. Lytken [97] F. Lyu [14a] V. Lyubushkin [38] T. Lyubushkina [38] H. Ma [29] L. L. Ma [62b] Y. Ma [95] D. M. Mac Donell [164] G. Maccarrone [53] J. C. MacDonald [138] R. Madar [40] W. F. Mader [50] J. Maeda [83] T. Maeno [29] M. Maerker [50] V. Magerl [54] H. Maguire [138] D. J. Mahon [41] C. Maidantchik [81b] A. Maio [129a,129b,129d] K. Maj [84a] O. Majersky [28a] S. Majewski [122] N. Makovec [66] V. Maksimovic [15] B. Malaescu [126] Pa. Malecki [85] V. P. Maleev [37] F. Malek [60] D. Malito [43b,43a] U. Mallik [79] C. Malone [32] S. Maltezos [10] S. Malyukov [38] J. Mamuzic [13] G. Mancini [53] G. Manco [72a,72b] J. P. Mandalia [93] I. Mandić [92] L. Manhaes de Andrade Filho [81a] I. M. Maniatis [151,ff] M. Manisha [134] J. Manjarres Ramos [50] D. C. Mankad [168] A. Mann [108] B. Mansoulie [134] S. Manzoni [36] A. Marantis [151,gg] G. Marchiori [5] M. Marcisovsky [130] L. Marcoccia [75a,75b] C. Marcon [70a,70b] M. Marinescu [20] M. Marjanovic [119] E. J. Marshall [90] Z. Marshall [17a] S. Marti-Garcia [162] T. A. Martin [166] V. J. Martin [52] B. Martin dit Latour [16] L. Martinelli [74a,74b] M. Martinez [13,z] P. Martinez Agullo [162] V. I. Martinez Outschoorn [102] P. Martinez Suarez [13] S. Martin-Haugh [133] V. S. Martoiu [27b] A. C. Martyniuk [95] A. Marzin [36] S. R. Maschek [109] L. Masetti [99] T. Mashimo [152] J. Masik [100] A. L. Maslennikov [37] L. Massa [23b] P. Massarotti [71a,71b] P. Mastrandrea [73a,73b] A. Mastroberardino [43b,43a] T. Masubuchi [152] T. Mathisen [160] N. Matsuzawa [152] J. Maurer [27b] B. Maček [92] D. A. Maximov [37] R. Mazini [147] I. Maznas [151,ff] M. Mazza [106] S. M. Mazza [135] C. Mc Ginn [29] J. P. Mc Gowan [103] S. P. Mc Kee [105] W. P. McCormack [17a] E. F. McDonald [104] A. E. McDougall [113] J. A. Mcfayden [145] G. Mchedlidze [148b] R. P. Mckenzie [33g] T. C. Mclachlan [48] D. J. Mclaughlin [95] K. D. McLean [164] S. J. McMahon [133] P. C. McNamara [104] C. M. Mcpartland [91] R. A. McPherson [164,q] T. Megy [40] S. Mehlhase [108] A. Mehta [91] B. Meirose [45] D. Melini [149] B. R. Mellado Garcia [33g] A. H. Melo [55] F. Meloni [48] E. D. Mendes Gouveia [129a] A. M. Mendes Jacques Da Costa [20] H. Y. Meng [154] L. Meng [90] S. Menke [109] M. Mentink [36] E. Meoni [43b,43a] C. Merlassino [125] L. Merola [71a,71b] C. Meroni [70a] G. Merz [105] O. Meshkov [37] J. K. R. Meshreki [140] J. Metcalfe [6] A. S. Mete [6] C. Meyer [67] J-P. Meyer [134] M. Michetti [18] R. P. Middleton [133] L. Mijović [52] G. Mikenberg [168] M. Mikestikova [130] M. Mikuž [92] H. Mildner [138] A. Milic [36] C. D. Milke [44] D. W. Miller [39] L. S. Miller [34] A. Milov [168] D. A. Milstead [47a,47b] T. Min [14c] A. A. Minaenko [37] I. A. Minashvili [148b] L. Mince [59] A. I. Mincer [116] B. Mindur [84a] M. Mineev [38] Y. Mino [86] L. M. Mir [13] M. Miralles Lopez [162] M. Mironova [125] M. C. Missio [112] T. Mitani [167] A. Mitra [166] V. A. Mitsou [162] O. Miu [154] P. S. Miyagawa [93] Y. Miyazaki [88] A. Mizukami [82] J. U. Mjörnmark [97] T. Mkrtchyan [63a] T. Mlinarevic [95] M. Mlynarikova [36] T. Moa [47a,47b] S. Mobius [55] K. Mochizuki [107] P. Moder [48] P. Mogg [108] A. F. Mohammed [14a,14d] S. Mohapatra [41] G. Mokgatitswane [33g] B. Mondal [140] S. Mondal [131] K. Mönig [48] E. Monnier [101] L. Monsonis Romero [162] J. Montejo Berlingen [36] M. Montella [118] F. Monticelli [89] N. Morange [66] A. L. Moreira De Carvalho [129a] M. Moreno Llácer [162] C. Moreno Martinez [56] P. Morettini [57b] S. Morgenstern [166] M. Morii [61] M. Morinaga [152] A. K. Morley [36] F. Morodei [74a,74b] L. Morvaj [36] P. Moschovakos [36] B. Moser [36] M. Mosidze [148b] T. Moskalets [54] P. Moskvitina [112] J. Moss [31,ii] E. J. W. Moyse [102] O. Mtintsilana [33g] S. Muanza [101] J. Mueller [128] D. Muenstermann [90] R. Müller [19] G. A. Mullier [160] J. J. Mullin [127] D. P. Mungo [154] J. L. Munoz Martinez [13] D. Munoz Perez [162] F. J. Munoz Sanchez [100] M. Murin [100] W. J. Murray [166,133] A. Murrone [70a,70b] J. M. Muse [119] M. Muškinja [17a] C. Mwewa [29] A. G. Myagkov [37,m] A. J. Myers [8] A. A. Myers [128] G. Myers [67] M. Myska [131] B. P. Nachman [17a] O. Nackenhorst [49] A. Nag [50] K. Nagai [125] K. Nagano [82] J. L. Nagle [29,i] E. Nagy [101] A. M. Nairz [36] Y. Nakahama [82] K. Nakamura [82] H. Nanjo [123] R. Narayan [44] E. A. Narayanan [111] I. Naryshkin [37] M. Naseri [34] C. Nass [24] G. Navarro [22a] J. Navarro-Gonzalez [162] R. Nayak [150] A. Nayaz [18] P. Y. Nechaeva [37] F. Nechansky [48] L. Nedic [125] T. J. Neep [20] A. Negri [72a,72b] M. Negrini [23b] C. Nellist [112] C. Nelson [103]

K. Nelson,[105] S. Nemecek,[130] M. Nessi,[36,jj] M. S. Neubauer,[161] F. Neuhaus,[99] J. Neundorf,[48] R. Newhouse,[163] P. R. Newman,[20] C. W. Ng,[128] Y. S. Ng,[18] Y. W. Y. Ng,[48] B. Ngair,[35e] H. D. N. Nguyen,[107] R. B. Nickerson,[125] R. Nicolaidou,[134] J. Nielsen,[135] M. Niemeyer,[55] N. Nikiforou,[36] V. Nikolaenko,[37,m] I. Nikolic-Audit,[126] K. Nikolopoulos,[20] P. Nilsson,[29] H. R. Nindhito,[56] A. Nisati,[74a] N. Nishu,[2] R. Nisius,[109] J-E. Nitschke,[50] E. K. Nkadimeng,[33g] S. J. Noacco Rosende,[89] T. Nobe,[152] D. L. Noel,[32] Y. Noguchi,[86] T. Nommensen,[146] M. A. Nomura,[29] M. B. Norfolk,[138] R. R. B. Norisam,[95] B. J. Norman,[34] J. Novak,[92] T. Novak,[48] O. Novgorodova,[50] L. Novotny,[131] R. Novotny,[111] L. Nozka,[121] K. Ntekas,[159] N. M. J. Nunes De Moura Junior,[81b] E. Nurse,[95] F. G. Oakham,[34,e] J. Ocariz,[126] A. Ochi,[83] I. Ochoa,[129a] S. Oerdek,[160] A. Ogrodnik,[84a] A. Oh,[100] C. C. Ohm,[143] H. Oide,[82] R. Oishi,[152] M. L. Ojeda,[48] Y. Okazaki,[86] M. W. O'Keefe,[91] Y. Okumura,[152] A. Olariu,[27b] L. F. Oleiro Seabra,[129a] S. A. Olivares Pino,[136e] D. Oliveira Damazio,[29] D. Oliveira Goncalves,[81a] J. L. Oliver,[159] M. J. R. Olsson,[159] A. Olszewski,[85] J. Olszowska,[85,a] Ö. O. Öncel,[54] D. C. O'Neil,[141] A. P. O'Neill,[19] A. Onofre,[129a,129e] P. U. E. Onyisi,[11] M. J. Oreglia,[39] G. E. Orellana,[89] D. Orestano,[76a,76b] N. Orlando,[13] R. S. Orr,[154] V. O'Shea,[59] R. Ospanov,[62a] G. Otero y Garzon,[30] H. Otono,[88] P. S. Ott,[63a] G. J. Ottino,[17a] M. Ouchrif,[35d] J. Ouellette,[29,i] F. Ould-Saada,[124] M. Owen,[59] R. E. Owen,[133] K. Y. Oyulmaz,[21a] V. E. Ozcan,[21a] N. Ozturk,[8] S. Ozturk,[21d] J. Pacalt,[121] H. A. Pacey,[32] K. Pachal,[51] A. Pacheco Pages,[13] C. Padilla Aranda,[13] G. Padovano,[74a,74b] S. Pagan Griso,[17a] G. Palacino,[67] A. Palazzo,[69a,69b] S. Palestini,[36] M. Palka,[84b] J. Pan,[171] T. Pan,[64a] D. K. Panchal,[11] C. E. Pandini,[113] J. G. Panduro Vazquez,[94] H. Pang,[14b] P. Pani,[48] G. Panizzo,[68a,68c] L. Paolozzi,[56] C. Papadatos,[107] S. Parajuli,[44] A. Paramonov,[6] C. Paraskevopoulos,[10] D. Paredes Hernandez,[64b] T. H. Park,[154] M. A. Parker,[32] F. Parodi,[57b,57a] E. W. Parrish,[114] V. A. Parrish,[52] J. A. Parsons,[41] U. Parzefall,[54] B. Pascual Dias,[107] L. Pascual Dominguez,[150] V. R. Pascuzzi,[17a] F. Pasquali,[113] E. Pasqualucci,[74a] S. Passaggio,[57b] F. Pastore,[94] P. Pasuwan,[47a,47b] P. Patel,[85] J. R. Pater,[100] T. Pauly,[36] J. Pearkes,[142] M. Pedersen,[124] R. Pedro,[129a] S. V. Peleganchuk,[37] O. Penc,[36] E. A. Pender,[52] C. Peng,[64b] H. Peng,[62a] K. E. Penski,[108] M. Penzin,[37] B. S. Peralva,[81d] A. P. Pereira Peixoto,[60] L. Pereira Sanchez,[47a,47b] D. V. Perepelitsa,[29,i] E. Perez Codina,[155a] M. Perganti,[10] L. Perini,[70a,70b,a] H. Pernegger,[36] S. Perrella,[36] A. Perrevoort,[112] O. Perrin,[40] K. Peters,[48] R. F. Y. Peters,[100] B. A. Petersen,[36] T. C. Petersen,[42] E. Petit,[101] V. Petousis,[131] C. Petridou,[151,ff] A. Petrukhin,[140] M. Pettee,[17a] N. E. Pettersson,[36] A. Petukhov,[37] K. Petukhova,[132] A. Peyaud,[134] R. Pezoa,[136f] L. Pezzotti,[36] G. Pezzullo,[171] T. M. Pham,[169] T. Pham,[104] P. W. Phillips,[133] M. W. Phipps,[161] G. Piacquadio,[144] E. Pianori,[17a] F. Piazza,[70a,70b] R. Piegaia,[30] D. Pietreanu,[27b] A. D. Pilkington,[100] M. Pinamonti,[68a,68c] J. L. Pinfold,[2] G. Pinheiro Matos,[41] B. C. Pinheiro Pereira,[129a] C. Pitman Donaldson,[95] D. A. Pizzi,[34] L. Pizzimento,[75a,75b] A. Pizzini,[113] M.-A. Pleier,[29] V. Plesanovs,[54] V. Pleskot,[132] E. Plotnikova,[38] G. Poddar,[4] R. Poettgen,[97] L. Poggioli,[126] I. Pogrebnyak,[106] D. Pohl,[24] I. Pokharel,[55] S. Polacek,[132] G. Polesello,[72a] A. Poley,[141,155a] R. Polifka,[131] A. Polini,[23b] C. S. Pollard,[125] Z. B. Pollock,[118] V. Polychronakos,[29] E. Pompa Pacchi,[74a,74b] D. Ponomarenko,[37] L. Pontecorvo,[36] S. Popa,[27a] G. A. Popeneciu,[27d] D. M. Portillo Quintero,[155a] S. Pospisil,[131] P. Postolache,[27c] K. Potamianos,[125] I. N. Potrap,[38] C. J. Potter,[32] H. Potti,[1] T. Poulsen,[48] J. Poveda,[162] M. E. Pozo Astigarraga,[36] A. Prades Ibanez,[162] M. M. Prapa,[46] J. Pretel,[54] D. Price,[100] M. Primavera,[69a] M. A. Principe Martin,[98] R. Privara,[121] M. L. Proffitt,[137] N. Proklova,[127] K. Prokofiev,[64c] G. Proto,[75a,75b] S. Protopopescu,[29] J. Proudfoot,[6] M. Przybycien,[84a] J. E. Puddefoot,[138] D. Pudzha,[37] P. Puzo,[66] D. Pyatiizbyantseva,[37] J. Qian,[105] D. Qichen,[100] Y. Qin,[100] T. Qiu,[93] A. Quadt,[55] M. Queitsch-Maitland,[100] G. Quetant,[56] G. Rabanal Bolanos,[61] D. Rafanoharana,[54] F. Ragusa,[70a,70b] J. L. Rainbolt,[39] J. A. Raine,[56] S. Rajagopalan,[29] E. Ramakoti,[37] K. Ran,[48,14d] N. P. Rapheeha,[33g] V. Raskina,[126] D. F. Rassloff,[63a] S. Rave,[99] B. Ravina,[55] I. Ravinovich,[168] M. Raymond,[36] A. L. Read,[124] N. P. Readioff,[138] D. M. Rebuzzi,[72a,72b] G. Redlinger,[29] K. Reeves,[45] J. A. Reidelsturz,[170] D. Reikher,[150] A. Reiss,[99] A. Rej,[140] C. Rembser,[36] A. Renardi,[48] M. Renda,[27b] M. B. Rendel,[109] F. Renner,[48] A. G. Rennie,[59] S. Resconi,[70a] M. Ressegotti,[57b,57a] E. D. Resseguie,[17a] S. Rettie,[36] J. G. Reyes Rivera,[106] B. Reynolds,[118] E. Reynolds,[17a] M. Rezaei Estabragh,[170] O. L. Rezanova,[37] P. Reznicek,[132] E. Ricci,[77a,77b] R. Richter,[109] S. Richter,[47a,47b] E. Richter-Was,[84b] M. Ridel,[126] P. Rieck,[116] P. Riedler,[36] M. Rijssenbeek,[144] A. Rimoldi,[72a,72b] M. Rimoldi,[48] L. Rinaldi,[23b,23a] T. T. Rinn,[29] M. P. Rinnagel,[108] G. Ripellino,[143] I. Riu,[13] P. Rivadeneira,[48] J. C. Rivera Vergara,[164] F. Rizatdinova,[120] E. Rizvi,[93] C. Rizzi,[56] B. A. Roberts,[166] B. R. Roberts,[17a] S. H. Robertson,[103,q] M. Robin,[48] D. Robinson,[32]

C. M. Robles Gajardo,[136f] M. Robles Manzano,[99] A. Robson,[59] A. Rocchi,[75a,75b] C. Roda,[73a,73b] S. Rodriguez Bosca,[63a] Y. Rodriguez Garcia,[22a] A. Rodriguez Rodriguez,[54] A. M. Rodríguez Vera,[155b] S. Roe,[36] J. T. Roemer,[159] A. R. Roepe-Gier,[119] J. Roggel,[170] O. Røhne,[124] R. A. Rojas,[164] B. Roland,[54] C. P. A. Roland,[67] J. Roloff,[29] A. Romaniouk,[37] E. Romano,[72a,72b] M. Romano,[23b] A. C. Romero Hernandez,[161] N. Rompotis,[91] L. Roos,[126] S. Rosati,[74a] B. J. Rosser,[39] E. Rossi,[4] E. Rossi,[71a,71b] L. P. Rossi,[57b] L. Rossini,[48] R. Rosten,[118] M. Rotaru,[27b] B. Rottler,[54] D. Rousseau,[66] D. Rousso,[32] G. Rovelli,[72a,72b] A. Roy,[161] A. Rozanov,[101] Y. Rozen,[149] X. Ruan,[33g] A. Rubio Jimenez,[162] A. J. Ruby,[91] V. H. Ruelas Rivera,[18] T. A. Ruggeri,[1] F. Rühr,[54] A. Ruiz-Martinez,[162] A. Rummler,[36] Z. Rurikova,[54] N. A. Rusakovich,[38] H. L. Russell,[164] J. P. Rutherfoord,[7] K. Rybacki,[90] M. Rybar,[132] E. B. Rye,[124] A. Ryzhov,[37] J. A. Sabater Iglesias,[56] P. Sabatini,[162] L. Sabetta,[74a,74b] H. F-W. Sadrozinski,[135] F. Safai Tehrani,[74a] B. Safarzadeh Samani,[145] M. Safdari,[142] S. Saha,[103] M. Sahinsoy,[109] M. Saimpert,[134] M. Saito,[152] T. Saito,[152] D. Salamani,[36] G. Salamanna,[76a,76b] A. Salnikov,[142] J. Salt,[162] A. Salvador Salas,[13] D. Salvatore,[43b,43a] F. Salvatore,[145] A. Salzburger,[36] D. Sammel,[54] D. Sampsonidis,[151,ff] D. Sampsonidou,[62d,62c] J. Sánchez,[162] A. Sanchez Pineda,[4] V. Sanchez Sebastian,[162] H. Sandaker,[124] C. O. Sander,[48] J. A. Sandesara,[102] M. Sandhoff,[170] C. Sandoval,[22b] D. P. C. Sankey,[133] A. Sansoni,[53] L. Santi,[74a,74b] C. Santoni,[40] H. Santos,[129a,129b] S. N. Santpur,[17a] A. Santra,[168] K. A. Saoucha,[138] J. G. Saraiva,[129a,129d] J. Sardain,[7] O. Sasaki,[82] K. Sato,[156] C. Sauer,[63b] F. Sauerburger,[54] E. Sauvan,[4] P. Savard,[154,e] R. Sawada,[152] C. Sawyer,[133] L. Sawyer,[96] I. Sayago Galvan,[162] C. Sbarra,[23b] A. Sbrizzi,[23b,23a] T. Scanlon,[95] J. Schaarschmidt,[137] P. Schacht,[109] D. Schaefer,[39] U. Schäfer,[99] A. C. Schaffer,[66] D. Schaile,[108] R. D. Schamberger,[144] E. Schanet,[108] C. Scharf,[18] M. M. Schefer,[19] V. A. Schegelsky,[37] D. Scheirich,[132] F. Schenck,[18] M. Schernau,[159] C. Scheulen,[55] C. Schiavi,[57b,57a] Z. M. Schillaci,[26] E. J. Schioppa,[69a,69b] M. Schioppa,[43b,43a] B. Schlag,[99] K. E. Schleicher,[54] S. Schlenker,[36] J. Schmeing,[170] M. A. Schmidt,[170] K. Schmieden,[99] C. Schmitt,[99] S. Schmitt,[48] L. Schoeffel,[134] A. Schoening,[63b] P. G. Scholer,[54] E. Schopf,[125] M. Schott,[99] J. Schovancova,[36] S. Schramm,[56] F. Schroeder,[170] H-C. Schultz-Coulon,[63a] M. Schumacher,[54] B. A. Schumm,[135] Ph. Schune,[134] A. Schwartzman,[142] T. A. Schwarz,[105] Ph. Schwemling,[134] R. Schwienhorst,[106] A. Sciandra,[135] G. Sciolla,[26] F. Scuri,[73a] F. Scutti,[104] C. D. Sebastiani,[91] K. Sedlaczek,[49] P. Seema,[18] S. C. Seidel,[111] A. Seiden,[135] B. D. Seidlitz,[41] T. Seiss,[39] C. Seitz,[48] J. M. Seixas,[81b] G. Sekhniaidze,[71a] S. J. Sekula,[44] L. Selem,[4] N. Semprini-Cesari,[23b,23a] S. Sen,[51] D. Sengupta,[56] V. Senthilkumar,[162] L. Serin,[66] L. Serkin,[68a,68b] M. Sessa,[76a,76b] H. Severini,[119] S. Sevova,[142] F. Sforza,[57b,57a] A. Sfyrla,[56] E. Shabalina,[55] R. Shaheen,[143] J. D. Shahinian,[127] D. Shaked Renous,[168] L. Y. Shan,[14a] M. Shapiro,[17a] A. Sharma,[36] A. S. Sharma,[163] P. Sharma,[79] S. Sharma,[48] P. B. Shatalov,[37] K. Shaw,[145] S. M. Shaw,[100] Q. Shen,[62c,5] P. Sherwood,[95] L. Shi,[95] C. O. Shimmin,[171] Y. Shimogama,[167] J. D. Shinner,[94] I. P. J. Shipsey,[125] S. Shirabe,[60] M. Shiyakova,[38,kk] J. Shlomi,[168] M. J. Shochet,[39] J. Shojaii,[104] D. R. Shope,[124] S. Shrestha,[118,ll] E. M. Shrif,[33g] M. J. Shroff,[164] P. Sicho,[130] A. M. Sickles,[161] E. Sideras Haddad,[33g] A. Sidoti,[23b] F. Siegert,[50] Dj. Sijacki,[15] R. Sikora,[84a] F. Sili,[89] J. M. Silva,[20] M. V. Silva Oliveira,[36] S. B. Silverstein,[47a] S. Simion,[66] R. Simoniello,[36] E. L. Simpson,[59] N. D. Simpson,[97] S. Simsek,[21d] S. Sindhu,[55] P. Sinervo,[154] V. Sinetckii,[37] S. Singh,[141] S. Singh,[154] S. Sinha,[48] S. Sinha,[33g] M. Sioli,[23b,23a] I. Siral,[36] S. Yu. Sivoklokov,[37,a] J. Sjölin,[47a,47b] A. Skaf,[55] E. Skorda,[97] P. Skubic,[119] M. Slawinska,[85] V. Smakhtin,[168] B. H. Smart,[133] J. Smiesko,[36] S. Yu. Smirnov,[37] Y. Smirnov,[37] L. N. Smirnova,[37,m] O. Smirnova,[97] A. C. Smith,[41] E. A. Smith,[39] H. A. Smith,[125] J. L. Smith,[91] R. Smith,[142] M. Smizanska,[90] K. Smolek,[131] A. Smykiewicz,[85] A. A. Snesarev,[37] H. L. Snoek,[113] S. Snyder,[29] R. Sobie,[164,q] A. Soffer,[150] C. A. Solans Sanchez,[36] E. Yu. Soldatov,[37] U. Soldevila,[162] A. A. Solodkov,[37] S. Solomon,[54] A. Soloshenko,[38] K. Solovieva,[54] O. V. Solovyanov,[37] V. Solovyev,[37] P. Sommer,[36] A. Sonay,[13] W. Y. Song,[155b] A. Sopczak,[131] A. L. Sopio,[95] F. Sopkova,[28b] V. Sothilingam,[63a] S. Sottocornola,[72a,72b] R. Soualah,[115b] Z. Soumaimi,[35e] D. South,[48] S. Spagnolo,[69a,69b] M. Spalla,[109] F. Spanò,[94] D. Sperlich,[54] G. Spigo,[36] M. Spina,[145] S. Spinali,[90] D. P. Spiteri,[59] M. Spousta,[132] E. J. Staats,[34] A. Stabile,[70a,70b] R. Stamen,[63a] M. Stamenkovic,[113] A. Stampekis,[20] M. Standke,[24] E. Stanecka,[85] M. V. Stange,[50] B. Stanislaus,[17a] M. M. Stanitzki,[48] M. Stankaityte,[125] B. Stapf,[48] E. A. Starchenko,[37] G. H. Stark,[135] J. Stark,[101,mm] D. M. Starko,[155b] P. Staroba,[130] P. Starovoitov,[63a] S. Stärz,[103] R. Staszewski,[85] G. Stavropoulos,[46] J. Steentoft,[160] P. Steinberg,[29] A. L. Steinhebel,[122] B. Stelzer,[141,155a] H. J. Stelzer,[128] O. Stelzer-Chilton,[155a] H. Stenzel,[58] T. J. Stevenson,[145] G. A. Stewart,[36] M. C. Stockton,[36] G. Stoicea,[27b] M. Stolarski,[129a]

S. Stonjek[109] A. Straessner[50] J. Strandberg[143] S. Strandberg[47a,47b] M. Strauss[119] T. Strebler[101]
P. Strizenec[28b] R. Ströhmer[165] D. M. Strom[122] L. R. Strom[48] R. Stroynowski[44] A. Strubig[47a,47b]
S. A. Stucci[29] B. Stugu[16] J. Stupak[119] N. A. Styles[48] D. Su[142] S. Su[62a] W. Su[62d,137,62c] X. Su[62a,66]
K. Sugizaki[152] V. V. Sulin[37] M. J. Sullivan[91] D. M. S. Sultan[77a,77b] L. Sultanaliyeva[37] S. Sultansoy[3b]
T. Sumida[86] S. Sun[105] S. Sun[169] O. Sunneborn Gudnadottir[160] M. R. Sutton[145] M. Svatos[130]
M. Swiatlowski[155a] T. Swirski[165] I. Sykora[28a] M. Sykora[132] T. Sykora[132] D. Ta[99] K. Tackmann[48,nn]
A. Taffard[159] R. Tafirout[155a] J. S. Tafoya Vargas[66] R. H. M. Taibah[126] R. Takashima[87] K. Takeda[83]
E. P. Takeva[52] Y. Takubo[82] M. Talby[101] A. A. Talyshev[37] K. C. Tam[64b] N. M. Tamir[150] A. Tanaka[152]
J. Tanaka[152] R. Tanaka[66] M. Tanasini[57b,57a] J. Tang[62c] Z. Tao[163] S. Tapia Araya[80] S. Tapprogge[99]
A. Tarek Abouelfadl Mohamed[106] S. Tarem[149] K. Tariq[62b] G. Tarna[101,27b] G. F. Tartarelli[70a] P. Tas[132]
M. Tasevsky[130] E. Tassi[43b,43a] A. C. Tate[161] G. Tateno[152] Y. Tayalati[35e] G. N. Taylor[104] W. Taylor[155b]
H. Teagle[91] A. S. Tee[169] R. Teixeira De Lima[142] P. Teixeira-Dias[94] J. J. Teoh[154] K. Terashi[152] J. Terron[98]
S. Terzo[13] M. Testa[53] R. J. Teuscher[154,q] A. Thaler[78] O. Theiner[56] N. Themistokleous[52]
T. Theveneaux-Pelzer[18] O. Thielmann[170] D. W. Thomas[94] J. P. Thomas[20] E. A. Thompson[48] P. D. Thompson[20]
E. Thomson[127] E. J. Thorpe[93] Y. Tian[55] V. Tikhomirov[37,m] Yu. A. Tikhonov[37] S. Timoshenko[37]
E. X. L. Ting[1] P. Tipton[171] S. Tisserant[101] S. H. Tlou[33g] A. Tnourji[40] K. Todome[23b,23a] S. Todorova-Nova[132]
S. Todt[50] M. Togawa[82] J. Tojo[88] S. Tokár[28a] K. Tokushuku[82] R. Tombs[32] M. Tomoto[82,110] L. Tompkins[142,w]
K. W. Topolnicki[84b] P. Tornambe[102] E. Torrence[122] H. Torres[50] E. Torró Pastor[162] M. Toscani[30] C. Tosciri[39]
M. Tost[11] D. R. Tovey[138] A. Traeet[16] I. S. Trandafir[27b] T. Trefzger[165] A. Tricoli[29] I. M. Trigger[155a]
S. Trincaz-Duvoid[126] D. A. Trischuk[26] B. Trocmé[60] A. Trofymov[66] C. Troncon[70a] L. Truong[33c]
M. Trzebinski[85] A. Trzupek[85] F. Tsai[144] M. Tsai[105] A. Tsiamis[151,ff] P. V. Tsiareshka[37] S. Tsigaridas[155a]
A. Tsirigotis[151,gg] V. Tsiskaridze[144] E. G. Tskhadadze[148a] M. Tsopoulou[151,ff] Y. Tsujikawa[86] I. I. Tsukerman[37]
V. Tsulaia[17a] S. Tsuno[82] O. Tsur[149] D. Tsybychev[144] Y. Tu[64b] A. Tudorache[27b] V. Tudorache[27b]
A. N. Tuna[36] S. Turchikhin[38] I. Turk Cakir[3a] R. Turra[70a] T. Turtuvshin[38,oo] P. M. Tuts[41] S. Tzamarias[151,ff]
P. Tzanis[10] E. Tzovara[99] K. Uchida[152] F. Ukegawa[156] P. A. Ulloa Poblete[136c] E. N. Umaka[80] G. Unal[36]
M. Unal[11] A. Undrus[29] G. Unel[159] J. Urban[28b] P. Urquijo[104] G. Usai[8] R. Ushioda[153] M. Usman[107]
Z. Uysal[21b] L. Vacavant[101] V. Vacek[131] B. Vachon[103] K. O. H. Vadla[124] T. Vafeiadis[36] A. Vaitkus[95]
C. Valderanis[108] E. Valdes Santurio[47a,47b] M. Valente[155a] S. Valentinetti[23b,23a] A. Valero[162] A. Vallier[101,mm]
J. A. Valls Ferrer[162] T. R. Van Daalen[137] P. Van Gemmeren[6] M. Van Rijnbach[124,36] S. Van Stroud[95]
I. Van Vulpen[113] M. Vanadia[75a,75b] W. Vandelli[36] M. Vandenbroucke[134] E. R. Vandewall[120] D. Vannicola[150]
L. Vannoli[57b,57a] R. Vari[74a] E. W. Varnes[7] C. Varni[17a] T. Varol[147] D. Varouchas[66] L. Varriale[162]
K. E. Varvell[146] M. E. Vasile[27b] L. Vaslin[40] G. A. Vasquez[164] F. Vazeille[40] T. Vazquez Schroeder[36] J. Veatch[31]
V. Vecchio[100] M. J. Veen[102] I. Veliscek[125] L. M. Veloce[154] F. Veloso[129a,129c] S. Veneziano[74a]
A. Ventura[69a,69b] A. Verbytskyi[109] M. Verducci[73a,73b] C. Vergis[24] M. Verissimo De Araujo[81b] W. Verkerke[113]
J. C. Vermeulen[113] C. Vernieri[142] P. J. Verschuuren[94] M. Vessella[102] M. C. Vetterli[141,e] A. Vgenopoulos[151,ff]
N. Viaux Maira[136f] T. Vickey[138] O. E. Vickey Boeriu[138] G. H. A. Viehhauser[125] L. Vigani[63b] M. Villa[23b,23a]
M. Villaplana Perez[162] E. M. Villhauer[52] E. Vilucchi[53] M. G. Vincter[34] G. S. Virdee[20] A. Vishwakarma[52]
C. Vittori[23b,23a] I. Vivarelli[145] V. Vladimirov[166] E. Voevodina[109] F. Vogel[108] P. Vokac[131] J. Von Ahnen[48]
E. Von Toerne[24] B. Vormwald[36] V. Vorobel[132] K. Vorobev[37] M. Vos[162] J. H. Vossebeld[91] M. Vozak[113]
L. Vozdecky[93] N. Vranjes[15] M. Vranjes Milosavljevic[15] M. Vreeswijk[113] R. Vuillermet[36] O. Vujinovic[99]
I. Vukotic[39] S. Wada[156] C. Wagner[102] W. Wagner[170] S. Wahdan[170] H. Wahlberg[89] R. Wakasa[156]
M. Wakida[110] V. M. Walbrecht[109] J. Walder[133] R. Walker[108] W. Walkowiak[140] A. M. Wang[61] A. Z. Wang[169]
C. Wang[62a] C. Wang[62c] H. Wang[17a] J. Wang[64a] R.-J. Wang[99] R. Wang[61] R. Wang[6] S. M. Wang[147]
S. Wang[62b] T. Wang[62a] W. T. Wang[79] X. Wang[14c] X. Wang[161] X. Wang[62c] Y. Wang[62d] Y. Wang[14c]
Z. Wang[105] Z. Wang[62d,51,62c] Z. Wang[105] A. Warburton[103] R. J. Ward[20] N. Warrack[59] A. T. Watson[20]
H. Watson[59] M. F. Watson[20] G. Watts[137] B. M. Waugh[95] A. F. Webb[11] C. Weber[29] H. A. Weber[18]
M. S. Weber[19] S. M. Weber[63a] C. Wei[62a] Y. Wei[125] A. R. Weidberg[125] J. Weingarten[49] M. Weirich[99]
C. Weiser[54] C. J. Wells[48] T. Wenaus[29] B. Wendland[49] T. Wengler[36] N. S. Wenke[109] N. Wermes[24]
M. Wessels[63a] K. Whalen[122] A. M. Wharton[90] A. S. White[61] A. White[8] M. J. White[1] D. Whiteson[159]

L. Wickremasinghe,[123] W. Wiedenmann,[169] C. Wiel,[50] M. Wielers,[133] N. Wieseotte,[99] C. Wiglesworth,[42]
L. A. M. Wiik-Fuchs,[54] D. J. Wilbern,[119] H. G. Wilkens,[36] D. M. Williams,[41] H. H. Williams,[127] S. Williams,[32]
S. Willocq,[102] P. J. Windischhofer,[125] F. Winklmeier,[122] B. T. Winter,[54] J. K. Winter,[100] M. Wittgen,[142]
M. Wobisch,[96] R. Wölker,[125] J. Wollrath,[159] M. W. Wolter,[85] H. Wolters,[129a,129c] V. W. S. Wong,[163]
A. F. Wongel,[48] S. D. Worm,[48] B. K. Wosiek,[85] K. W. Woźniak,[85] K. Wraight,[59] J. Wu,[14a,14d] M. Wu,[64a]
M. Wu,[112] S. L. Wu,[169] X. Wu,[56] Y. Wu,[62a] Z. Wu,[134,62a] J. Wuerzinger,[125] T. R. Wyatt,[100] B. M. Wynne,[52]
S. Xella,[42] L. Xia,[14c] M. Xia,[14b] J. Xiang,[64c] X. Xiao,[105] M. Xie,[62a] X. Xie,[62a] S. Xin,[14a,14d] J. Xiong,[17a]
I. Xiotidis,[145] D. Xu,[14a] H. Xu,[62a] H. Xu,[62a] L. Xu,[62a] R. Xu,[127] T. Xu,[105] W. Xu,[105] Y. Xu,[14b] Z. Xu,[62b]
Z. Xu,[14a] B. Yabsley,[146] S. Yacoob,[33a] N. Yamaguchi,[88] Y. Yamaguchi,[153] H. Yamauchi,[156] T. Yamazaki,[17a]
Y. Yamazaki,[83] J. Yan,[62c] S. Yan,[125] Z. Yan,[25] H. J. Yang,[62c,62d] H. T. Yang,[62a] S. Yang,[62a] T. Yang,[64c]
X. Yang,[62a] X. Yang,[14a] Y. Yang,[44] Z. Yang,[62a,105] W-M. Yao,[17a] Y. C. Yap,[48] H. Ye,[14c] H. Ye,[55] J. Ye,[44]
S. Ye,[29] X. Ye,[62a] Y. Yeh,[95] I. Yeletskikh,[38] B. K. Yeo,[17a] M. R. Yexley,[90] P. Yin,[41] K. Yorita,[167] S. Younas,[27b]
C. J. S. Young,[54] C. Young,[142] M. Yuan,[105] R. Yuan,[62b,pp] L. Yue,[95] X. Yue,[63a] M. Zaazoua,[35e] B. Zabinski,[85]
E. Zaid,[52] T. Zakareishvili,[148b] N. Zakharchuk,[34] S. Zambito,[56] J. A. Zamora Saa,[136d,136b] J. Zang,[152] D. Zanzi,[54]
O. Zaplatilek,[131] S. V. Zeißner,[49] C. Zeitnitz,[170] J. C. Zeng,[161] D. T. Zenger Jr.,[26] O. Zenin,[37] T. Ženiš,[28a]
S. Zenz,[93] S. Zerradi,[35a] D. Zerwas,[66] B. Zhang,[14c] D. F. Zhang,[138] G. Zhang,[14b] J. Zhang,[62b] J. Zhang,[6]
K. Zhang,[14a,14d] L. Zhang,[14c] P. Zhang,[14a,14d] R. Zhang,[169] S. Zhang,[105] T. Zhang,[152] X. Zhang,[62c] X. Zhang,[62b]
Y. Zhang,[62c,5] Z. Zhang,[17a] Z. Zhang,[66] H. Zhao,[137] P. Zhao,[51] T. Zhao,[62b] Y. Zhao,[135] Z. Zhao,[62a]
A. Zhemchugov,[38] X. Zheng,[62a] Z. Zheng,[142] D. Zhong,[161] B. Zhou,[105] C. Zhou,[169] H. Zhou,[7] N. Zhou,[62c]
Y. Zhou,[7] C. G. Zhu,[62b] C. Zhu,[14a,14d] H. L. Zhu,[62a] H. Zhu,[14a] J. Zhu,[105] Y. Zhu,[62c] Y. Zhu,[62a] X. Zhuang,[14a]
K. Zhukov,[37] V. Zhulanov,[37] N. I. Zimine,[38] J. Zinsser,[63b] M. Ziolkowski,[140] L. Živković,[15] A. Zoccoli,[23b,23a]
K. Zoch,[56] T. G. Zorbas,[138] O. Zormpa,[46] W. Zou,[41] and L. Zwalinski[36]

(ATLAS Collaboration)

[1]*Department of Physics, University of Adelaide, Adelaide South Australia, Australia*
[2]*Department of Physics, University of Alberta, Edmonton Alberta, Canada*
[3a]*Department of Physics, Ankara University, Ankara, Türkiye*
[3b]*Division of Physics, TOBB University of Economics and Technology, Ankara, Türkiye*
[4]*LAPP, Université Savoie Mont Blanc, CNRS/IN2P3, Annecy, France*
[5]*APC, Université Paris Cité, CNRS/IN2P3, Paris, France*
[6]*High Energy Physics Division, Argonne National Laboratory, Argonne Illinois, USA*
[7]*Department of Physics, University of Arizona, Tucson Arizona, USA*
[8]*Department of Physics, University of Texas at Arlington, Arlington Texas, USA*
[9]*Physics Department, National and Kapodistrian University of Athens, Athens, Greece*
[10]*Physics Department, National Technical University of Athens, Zografou, Greece*
[11]*Department of Physics, University of Texas at Austin, Austin Texas, USA*
[12]*Institute of Physics, Azerbaijan Academy of Sciences, Baku, Azerbaijan*
[13]*Institut de Física d'Altes Energies (IFAE), Barcelona Institute of Science and Technology,
Barcelona, Spain*
[14a]*Institute of High Energy Physics, Chinese Academy of Sciences, Beijing, China*
[14b]*Physics Department, Tsinghua University, Beijing, China*
[14c]*Department of Physics, Nanjing University, Nanjing, China*
[14d]*University of Chinese Academy of Science (UCAS), Beijing, China*
[15]*Institute of Physics, University of Belgrade, Belgrade, Serbia*
[16]*Department for Physics and Technology, University of Bergen, Bergen, Norway*
[17a]*Physics Division, Lawrence Berkeley National Laboratory, Berkeley California, USA*
[17b]*University of California, Berkeley California, USA*
[18]*Institut für Physik, Humboldt Universität zu Berlin, Berlin, Germany*
[19]*Albert Einstein Center for Fundamental Physics and Laboratory for High Energy Physics,
University of Bern, Bern, Switzerland*
[20]*School of Physics and Astronomy, University of Birmingham, Birmingham, United Kingdom*
[21a]*Department of Physics, Bogazici University, Istanbul, Türkiye*
[21b]*Department of Physics Engineering, Gaziantep University, Gaziantep, Türkiye*
[21c]*Department of Physics, Istanbul University, Istanbul, Türkiye*

[21d]*Istinye University, Sariyer, Istanbul, Türkiye*

[22a]*Facultad de Ciencias y Centro de Investigaciónes, Universidad Antonio Nariño, Bogotá, Colombia*

[22b]*Departamento de Física, Universidad Nacional de Colombia, Bogotá, Colombia*

[23a]*Dipartimento di Fisica e Astronomia A. Righi, Università di Bologna, Bologna, Italy*

[23b]*INFN Sezione di Bologna, Italy*

[24]*Physikalisches Institut, Universität Bonn, Bonn, Germany*

[25]*Department of Physics, Boston University, Boston Massachusetts. UA*

[26]*Department of Physics, Brandeis University, Waltham Massachusetts. UA*

[27a]*Transilvania University of Brasov, Brasov, Romania*

[27b]*Horia Hulubei National Institute of Physics and Nuclear Engineering, Bucharest, Romania*

[27c]*Department of Physics, Alexandru Ioan Cuza University of Iasi, Iasi, Romania*

[27d]*National Institute for Research and Development of Isotopic and Molecular Technologies, Physics Department, Cluj-Napoca, Romania*

[27e]*University Politehnica Bucharest, Bucharest, Romania*

[27f]*West University in Timisoara, Timisoara, Romania*

[27g]*Faculty of Physics, University of Bucharest, Bucharest, Romania*

[28a]*Faculty of Mathematics, Physics and Informatics, Comenius University, Bratislava, Slovak Republic*

[28b]*Department of Subnuclear Physics, Institute of Experimental Physics of the Slovak Academy of Sciences, Kosice, Slovak Republic*

[29]*Physics Department, Brookhaven National Laboratory, Upton New York, USA*

[30]*Universidad de Buenos Aires, Facultad de Ciencias Exactas y Naturales, Departamento de Física, y CONICET, Instituto de Física de Buenos Aires (IFIBA), Buenos Aires, Argentina*

[31]*California State University, California, USA*

[32]*Cavendish Laboratory, University of Cambridge, Cambridge, United Kingdom*

[33a]*Department of Physics, University of Cape Town, Cape Town, South Africa*

[33b]*iThemba Labs, Western Cape, South Africa*

[33c]*Department of Mechanical Engineering Science, University of Johannesburg, Johannesburg, South Africa*

[33d]*National Institute of Physics, University of the Philippines Diliman (Philippines), Philippines*

[33e]*University of South Africa, Department of Physics, Pretoria, South Africa*

[33f]*University of Zululand, KwaDlangezwa, South Africa*

[33g]*School of Physics, University of the Witwatersrand, Johannesburg, South Africa*

[34]*Department of Physics, Carleton University, Ottawa ON, Canada*

[35a]*Faculté des Sciences Ain Chock, Réseau Universitaire de Physique des Hautes Energies—Université Hassan II, Casablanca, Morocco*

[35b]*Faculté des Sciences, Université Ibn-Tofail, Kénitra, Morocco*

[35c]*Faculté des Sciences Semlalia, Université Cadi Ayyad, LPHEA-Marrakech, Morocco*

[35d]*LPMR, Faculté des Sciences, Université Mohamed Premier, Oujda, Morocco*

[35e]*Faculté des sciences, Université Mohammed V, Rabat, Morocco*

[35f]*Institute of Applied Physics, Mohammed VI Polytechnic University, Ben Guerir, Morocco*

[36]*CERN, Geneva, Switzerland*

[37]*Affiliated with an institute covered by a cooperation agreement with CERN*

[38]*Affiliated with an international laboratory covered by a cooperation agreement with CERN*

[39]*Enrico Fermi Institute, University of Chicago, Chicago Illinois, USA*

[40]*LPC, Université Clermont Auvergne, CNRS/IN2P3, Clermont-Ferrand, France*

[41]*Nevis Laboratory, Columbia University, Irvington New York, USA*

[42]*Niels Bohr Institute, University of Copenhagen, Copenhagen, Denmark*

[43a]*Dipartimento di Fisica, Università della Calabria, Rende, Italy*

[43b]*INFN Gruppo Collegato di Cosenza, Laboratori Nazionali di Frascati, Italy*

[44]*Physics Department, Southern Methodist University, Dallas Texas, USA*

[45]*Physics Department, University of Texas at Dallas, Richardson Texas, USA*

[46]*National Centre for Scientific Research "Demokritos", Agia Paraskevi, Greece*

[47a]*Department of Physics, Stockholm University, Sweden*

[47b]*Oskar Klein Centre, Stockholm, Sweden*

[48]*Deutsches Elektronen-Synchrotron DESY, Hamburg and Zeuthen, Germany*

[49]*Fakultät Physik, Technische Universität Dortmund, Dortmund, Germany*

[50]*Institut für Kern- und Teilchenphysik, Technische Universität Dresden, Dresden, Germany*

[51]*Department of Physics, Duke University, Durham North Carolina, USA*

[52]*SUPA—School of Physics and Astronomy, University of Edinburgh, Edinburgh, United Kingdom*

[53]*INFN e Laboratori Nazionali di Frascati, Frascati, Italy*

[54]*Physikalisches Institut, Albert-Ludwigs-Universität Freiburg, Freiburg, Germany*

[55]*II. Physikalisches Institut, Georg-August-Universität Göttingen, Göttingen, Germany*

[56]*Département de Physique Nucléaire et Corpusculaire, Université de Genève, Genève, Switzerland*

[57a]*Dipartimento di Fisica, Università di Genova, Genova, Italy*

[57b]*INFN Sezione di Genova, Italy*

[58]*II. Physikalisches Institut, Justus-Liebig-Universität Giessen, Giessen, Germany*

[59]*SUPA—School of Physics and Astronomy, University of Glasgow, Glasgow, United Kingdom*

[60]*LPSC, Université Grenoble Alpes, CNRS/IN2P3, Grenoble INP, Grenoble, France*

[61]*Laboratory for Particle Physics and Cosmology, Harvard University, Cambridge Massachusetts, USA*

[62a]*Department of Modern Physics and State Key Laboratory of Particle Detection and Electronics, University of Science and Technology of China, Hefei, China*

[62b]*Institute of Frontier and Interdisciplinary Science and Key Laboratory of Particle Physics and Particle Irradiation (MOE), Shandong University, Qingdao, China*

[62c]*School of Physics and Astronomy, Shanghai Jiao Tong University, Key Laboratory for Particle Astrophysics and Cosmology (MOE), SKLPPC, Shanghai, China*

[62d]*Tsung-Dao Lee Institute, Shanghai, China*

[63a]*Kirchhoff-Institut für Physik, Ruprecht-Karls-Universität Heidelberg, Heidelberg, Germany*

[63b]*Physikalisches Institut, Ruprecht-Karls-Universität Heidelberg, Heidelberg, Germany*

[64a]*Department of Physics, Chinese University of Hong Kong, Shatin, N.T., Hong Kong, China*

[64b]*Department of Physics, University of Hong Kong, Hong Kong, China*

[64c]*Department of Physics and Institute for Advanced Study, Hong Kong University of Science and Technology, Clear Water Bay, Kowloon, Hong Kong, China*

[65]*Department of Physics, National Tsing Hua University, Hsinchu, Taiwan*

[66]*IJCLab, Université Paris-Saclay, CNRS/IN2P3, 91405, Orsay, France*

[67]*Department of Physics, Indiana University, Bloomington Indiana, USA*

[68a]*INFN Gruppo Collegato di Udine, Sezione di Trieste, Udine, Italy*

[68b]*ICTP, Trieste, Italy*

[68c]*Dipartimento Politecnico di Ingegneria e Architettura, Università di Udine, Udine, Italy*

[69a]*INFN Sezione di Lecce, Italy*

[69b]*Dipartimento di Matematica e Fisica, Università del Salento, Lecce, Italy*

[70a]*INFN Sezione di Milano, Italy*

[70b]*Dipartimento di Fisica, Università di Milano, Milano, Italy*

[71a]*INFN Sezione di Napoli, Italy*

[71b]*Dipartimento di Fisica, Università di Napoli, Napoli, Italy*

[72a]*INFN Sezione di Pavia, Italy*

[72b]*Dipartimento di Fisica, Università di Pavia, Pavia, Italy*

[73a]*INFN Sezione di Pisa, Italy*

[73b]*Dipartimento di Fisica E. Fermi, Università di Pisa, Pisa, Italy*

[74a]*INFN Sezione di Roma, Italy*

[74b]*Dipartimento di Fisica, Sapienza Università di Roma, Roma, Italy*

[75a]*INFN Sezione di Roma Tor Vergata, Italy*

[75b]*Dipartimento di Fisica, Università di Roma Tor Vergata, Roma, Italy*

[76a]*INFN Sezione di Roma Tre, Italy*

[76b]*Dipartimento di Matematica e Fisica, Università Roma Tre, Roma, Italy*

[77a]*INFN-TIFPA, Italy*

[77b]*Università degli Studi di Trento, Trento, Italy*

[78]*Universität Innsbruck, Department of Astro and Particle Physics, Innsbruck, Austria*

[79]*University of Iowa, Iowa City Iowa, USA*

[80]*Department of Physics and Astronomy, Iowa State University, Ames Iowa, USA*

[81a]*Departamento de Engenharia Elétrica, Universidade Federal de Juiz de Fora (UFJF), Juiz de Fora, Brazil*

[81b]*Universidade Federal do Rio De Janeiro COPPE/EE/IF, Rio de Janeiro, Brazil*

[81c]*Instituto de Física, Universidade de São Paulo, São Paulo, Brazil*

[81d]*Rio de Janeiro State University, Rio de Janeiro, Brazil*

[82]*KEK, High Energy Accelerator Research Organization, Tsukuba, Japan*

[83]*Graduate School of Science, Kobe University, Kobe, Japan*

[84a]*AGH University of Krakow, Faculty of Physics and Applied Computer Science, Krakow, Poland*

[84b]*Marian Smoluchowski Institute of Physics, Jagiellonian University, Krakow, Poland*

[85]*Institute of Nuclear Physics Polish Academy of Sciences, Krakow, Poland*

[86]*Faculty of Science, Kyoto University, Kyoto, Japan*

[87]*Kyoto University of Education, Kyoto, Japan*

[88]*Research Center for Advanced Particle Physics and Department of Physics, Kyushu University, Fukuoka, Japan*

[89]*Instituto de Física La Plata, Universidad Nacional de La Plata and CONICET, La Plata, Argentina*

[90]*Physics Department, Lancaster University, Lancaster, United Kingdom*

[91]*Oliver Lodge Laboratory, University of Liverpool, Liverpool, United Kingdom*

[92]*Department of Experimental Particle Physics, Jožef Stefan Institute and Department of Physics, University of Ljubljana, Ljubljana, Slovenia*

[93]*School of Physics and Astronomy, Queen Mary University of London, London, United Kingdom*

[94]*Department of Physics, Royal Holloway University of London, Egham, United Kingdom*

[95]*Department of Physics and Astronomy, University College London, London, United Kingdom*

[96]*Louisiana Tech University, Ruston Los Angeles, USA*

[97]*Fysiska institutionen, Lunds universitet, Lund, Sweden*

[98]*Departamento de Física Teorica C-15 and CIAFF, Universidad Autónoma de Madrid, Madrid, Spain*

[99]*Institut für Physik, Universität Mainz, Mainz, Germany*

[100]*School of Physics and Astronomy, University of Manchester, Manchester, United Kingdom*

[101]*CPPM, Aix-Marseille Université, CNRS/IN2P3, Marseille, France*

[102]*Department of Physics, University of Massachusetts, Amherst Massachusetts, USA*

[103]*Department of Physics, McGill University, Montreal Quebec, Canada*

[104]*School of Physics, University of Melbourne, Victoria, Australia*

[105]*Department of Physics, University of Michigan, Ann Arbor Michigan, USA*

[106]*Department of Physics and Astronomy, Michigan State University, East Lansing Michigan, USA*

[107]*Group of Particle Physics, University of Montreal, Montreal Quebec, Canada*

[108]*Fakultät für Physik, Ludwig-Maximilians-Universität München, München, Germany*

[109]*Max-Planck-Institut für Physik (Werner-Heisenberg-Institut), München, Germany*

[110]*Graduate School of Science and Kobayashi-Maskawa Institute, Nagoya University, Nagoya, Japan*

[111]*Department of Physics and Astronomy, University of New Mexico, Albuquerque New Mexico, USA*

[112]*Institute for Mathematics, Astrophysics and Particle Physics, Radboud University/Nikhef, Nijmegen, Netherlands*

[113]*Nikhef National Institute for Subatomic Physics and University of Amsterdam, Amsterdam, Netherlands*

[114]*Department of Physics, Northern Illinois University, DeKalb Illinois, USA*

[115a]*New York University Abu Dhabi, Abu Dhabi, United Arab Emirates*

[115b]*University of Sharjah, Sharjah, United Arab Emirates*

[116]*Department of Physics, New York University, New York New York, USA*

[117]*Ochanomizu University, Otsuka, Bunkyo-ku, Tokyo, Japan*

[118]*Ohio State University, Columbus Ohio, USA*

[119]*Homer L. Dodge Department of Physics and Astronomy, University of Oklahoma, Norman Oklahoma, USA*

[120]*Department of Physics, Oklahoma State University, Stillwater Oklahoma, USA*

[121]*Palacký University, Joint Laboratory of Optics, Olomouc, Czech Republic*

[122]*Institute for Fundamental Science, University of Oregon, Eugene, Oregon, USA*

[123]*Graduate School of Science, Osaka University, Osaka, Japan*

[124]*Department of Physics, University of Oslo, Oslo, Norway*

[125]*Department of Physics, Oxford University, Oxford, United Kingdom*

[126]*LPNHE, Sorbonne Université, Université Paris Cité, CNRS/IN2P3, Paris, France*

[127]*Department of Physics, University of Pennsylvania, Philadelphia Pennsylvania, USA*

[128]*Department of Physics and Astronomy, University of Pittsburgh, Pittsburgh Pennsylvania, USA*

[129a]*Laboratório de Instrumentação e Física Experimental de Partículas—LIP, Lisboa, Portugal*

[129b]*Departamento de Física, Faculdade de Ciências, Universidade de Lisboa, Lisboa, Portugal*

[129c]*Departamento de Física, Universidade de Coimbra, Coimbra, Portugal*

[129d]*Centro de Física Nuclear da Universidade de Lisboa, Lisboa, Portugal*

[129e]*Departamento de Física, Universidade do Minho, Braga, Portugal*

[129f]*Departamento de Física Teórica y del Cosmos, Universidad de Granada, Granada (Spain), Spain*

[129g]*Departamento de Física, Instituto Superior Técnico, Universidade de Lisboa, Lisboa, Portugal*

[130]*Institute of Physics of the Czech Academy of Sciences, Prague, Czech Republic*

[131]*Czech Technical University in Prague, Prague, Czech Republic*

[132]*Charles University, Faculty of Mathematics and Physics, Prague, Czech Republic*

[133]*Particle Physics Department, Rutherford Appleton Laboratory, Didcot, United Kingdom*

[134]*IRFU, CEA, Université Paris-Saclay, Gif-sur-Yvette, France*

[135]*Santa Cruz Institute for Particle Physics, University of California Santa Cruz, Santa Cruz California, USA*

[136a]*Departamento de Física, Pontificia Universidad Católica de Chile, Santiago, Chile*

[136b]*Millennium Institute for Subatomic physics at high energy frontier (SAPHIR), Santiago, Chile*

[136c]*Instituto de Investigación Multidisciplinario en Ciencia y Tecnología, y Departamento de Física, Universidad de La Serena, Chile*

[136d]*Universidad Andres Bello, Department of Physics, Santiago, Chile*

[136e]*Instituto de Alta Investigación, Universidad de Tarapacá, Arica, Chile*

[136f]*Departamento de Física, Universidad Técnica Federico Santa María, Valparaíso, Chile*

[137]*Department of Physics, University of Washington, Seattle Washington, USA*

[138]*Department of Physics and Astronomy, University of Sheffield, Sheffield, United Kingdom*

[139]*Department of Physics, Shinshu University, Nagano, Japan*

[140]*Department Physik, Universität Siegen, Siegen, Germany*

[141]*Department of Physics, Simon Fraser University, Burnaby British Columbia, Canada*

[142]*SLAC National Accelerator Laboratory, Stanford California, USA*

[143]*Department of Physics, Royal Institute of Technology, Stockholm, Sweden*

[144]*Departments of Physics and Astronomy, Stony Brook University, Stony Brook New York, USA*

[145]*Department of Physics and Astronomy, University of Sussex, Brighton, United Kingdom*

[146]*School of Physics, University of Sydney, Sydney, New South Wales, Australia*

[147]*Institute of Physics, Academia Sinica, Taipei, Taiwan*

[148a]*E. Andronikashvili Institute of Physics, Iv. Javakhishvili Tbilisi State University, Tbilisi, Georgia*

[148b]*High Energy Physics Institute, Tbilisi State University, Tbilisi, Georgia*

[148c]*University of Georgia, Tbilisi, Georgia*

[149]*Department of Physics, Technion, Israel Institute of Technology, Haifa, Israel*

[150]*Raymond and Beverly Sackler School of Physics and Astronomy, Tel Aviv University, Tel Aviv, Israel*

[151]*Department of Physics, Aristotle University of Thessaloniki, Thessaloniki, Greece*

[152]*International Center for Elementary Particle Physics and Department of Physics, University of Tokyo, Tokyo, Japan*

[153]*Department of Physics, Tokyo Institute of Technology, Tokyo, Japan*

[154]*Department of Physics, University of Toronto, Toronto Ontario, Canada*

[155a]*TRIUMF, Vancouver BC, Canada*

[155b]*Department of Physics and Astronomy, York University, Toronto Ontario, Canada*

[156]*Division of Physics and Tomonaga Center for the History of the Universe, Faculty of Pure and Applied Sciences, University of Tsukuba, Tsukuba, Japan*

[157]*Department of Physics and Astronomy, Tufts University, Medford Massachusetts, USA*

[158]*United Arab Emirates University, Al Ain, United Arab Emirates*

[159]*Department of Physics and Astronomy, University of California Irvine, Irvine California, USA*

[160]*Department of Physics and Astronomy, University of Uppsala, Uppsala, Sweden*

[161]*Department of Physics, University of Illinois, Urbana Illinois, USA*

[162]*Instituto de Física Corpuscular (IFIC), Centro Mixto Universidad de Valencia—CSIC, Valencia, Spain*

[163]*Department of Physics, University of British Columbia, Vancouver British Columbia Canadian Province, Canada*

[164]*Department of Physics and Astronomy, University of Victoria, Victoria British Columbia Canadian Province, Canada*

[165]*Fakultät für Physik und Astronomie, Julius-Maximilians-Universität Würzburg, Würzburg, Germany*

[166]*Department of Physics, University of Warwick, Coventry, United Kingdom*

[167]*Waseda University, Tokyo, Japan*

[168]*Department of Particle Physics and Astrophysics, Weizmann Institute of Science, Rehovot, Israel*

[169]*Department of Physics, University of Wisconsin, Madison Wisconsin, USA*

[170]*Fakultät für Mathematik und Naturwissenschaften, Fachgruppe Physik, Bergische Universität Wuppertal, Wuppertal, Germany*

[171]*Department of Physics, Yale University, New Haven Connecticut, USA*

[a]Deceased.

[b]Also at Department of Physics, King's College London, London, United Kingdom.

[c]Also at Institute of Physics, Azerbaijan Academy of Sciences, Baku, Azerbaijan.

[d]Also at Lawrence Livermore National Laboratory, Livermore California, USA.

[e]Also at TRIUMF, Vancouver British Columbia, Canada.

[f]Also at Department of Physics, University of Thessaly, Greece.

[g]Also at An-Najah National University, Nablus, Palestine.

[h]Also at Department of Physics, University of Fribourg, Fribourg, Switzerland.
[i]Also at University of Colorado Boulder, Department of Physics, Colorado, USA.
[j]Also at Department of Physics and Astronomy, University of Louisville, Louisville, Kentucky, USA.
[k]Also at Department of Physics, Westmont College, Santa Barbara California, USA.
[l]Also at Departament de Fisica de la Universitat Autonoma de Barcelona, Barcelona, Spain.
[m]Also at Affiliated with an institute covered by a cooperation agreement with CERN.
[n]Also at The Collaborative Innovation Center of Quantum Matter (CICQM), Beijing, China.
[o]Also at Department of Physics, Ben Gurion University of the Negev, Beer Sheva, Israel.
[p]Also at Università di Napoli Parthenope, Napoli, Italy.
[q]Also at Institute of Particle Physics (IPP), Canada.
[r]Also at Bruno Kessler Foundation, Trento, Italy.
[s]Also at RWTH Aachen University, III. Physikalisches Institut A, Aachen, Germany.
[t]Also at Borough of Manhattan Community College, City University of New York, New York New York, USA.
[u]Also at National Institute of Physics, University of the Philippines Diliman (Philippines), Philippines.
[v]Also at Department of Financial and Management Engineering, University of the Aegean, Chios, Greece.
[w]Also at Department of Physics, Stanford University, Stanford California, USA.
[x]Also at Centro Studi e Ricerche Enrico Fermi, Italy.
[y]Also at Department of Physics, California State University, East Bay California, USA.
[z]Also at Institucio Catalana de Recerca i Estudis Avancats, ICREA, Barcelona, Spain.
[aa]Also at Technical University of Munich, Munich, Germany.
[bb]Also at University of Chinese Academy of Sciences (UCAS), Beijing, China.
[cc]Also at Yeditepe University, Physics Department, Istanbul, Türkiye.
[dd]Also at Institute of Theoretical Physics, Ilia State University, Tbilisi, Georgia.
[ee]Also at CERN, Geneva, Switzerland.
[ff]Also at Center for Interdisciplinary Research and Innovation (CIRI-AUTH), Thessaloniki, Greece.
[gg]Also at Hellenic Open University, Patras, Greece.
[hh]Also at Center for High Energy Physics, Peking University, China.
[ii]Also at Department of Physics, California State University, Sacramento California, USA.
[jj]Also at Département de Physique Nucléaire et Corpusculaire, Université de Genève, Genève, Switzerland.
[kk]Also at Institute for Nuclear Research and Nuclear Energy (INRNE) of the Bulgarian Academy of Sciences, Sofia, Bulgaria.
[ll]Also at Washington College, Maryland, USA.
[mm]Also at L2IT, Université de Toulouse, CNRS/IN2P3, UPS, Toulouse, France.
[nn]Also at Institut für Experimentalphysik, Universität Hamburg, Hamburg, Germany.
[oo]Also at Institute of Physics and Technology, Ulaanbaatar, Mongolia.
[pp]Also at Department of Physics and Astronomy, Michigan State University, East Lansing Michigan, USA.